ANALYZING THE ACCURACY OF ESTIMATES OF DENTAL CURING LIGHT DEGRADATION FROM CELL PHONE IMAGES

by

Yan Chang

Submitted in partial fulfillment of the requirements
for the degree of Master of Computer Science

at

Dalhousie University
Halifax, Nova Scotia
April 2020

Table of Contents

List of Tables

List of Figures

Abstract

Modern dentistry uses light-curing resin-based composites as restorative/filling materials. The LCU (dental light curing unit) is a device emitting blue light or a combination of blue and ultraviolet light to be placed directly over the tooth to harden the resin-based material in it. The curing effect depends on the irradiance and the time the material is exposed to the light. The LCU output light intensity degrades over time and with usage. Thus, curing times need to be updated accordingly to avoid an under-curing or over-curing process. Measuring the irradiance is a challenging task that is currently performed by trained professionals and laboratory grade spectrometers that are not cheap or portable. Dental clinics have to rely on measurements done by external consultants. But it is not usually possible for them to do the measurements frequently. Between two measurements, the light output of LCUs can deteriorate significantly and curing with inadequate time would result in restoration failures. This gives rise to the need for a low-cost, portable device that allows dentists to measure the degradation in the output of any LCU routinely. To study the effect of using cell phones for monitoring the LCU's degradation, this thesis uses different modes of an LCU to simulate the degradation and use the readings of an existing LCU calibration equipment as the baseline to evaluate the result from the analysis of the cell phone images. We capture the light source images for five different LCUs and calculate the total pixel intensity of the light foreground in the image to estimate the irradiance. We compare the raw images of DNG format and the images of JPG format in terms of relative error and overall variation on different aspects and conclude that for the data considered, the raw images provide superior accuracy in the case of poorly chosen exposure times.

List of Abbreviations Used

API	Application programming interface
CCD	Charge-coupled devices
CFA	Color filter array
CMOS	Complementary metal oxide semiconductors
CQ	Camphorquinone
CV	Coefficient of variation
DNG	Digital negative
GIF	Graphics Interchange Format
IFDs	Image file directories
JPG	Joint photographic experts group
LCU	Dental light curing unit
LED	Laser and light emitting diodes
ND	Neutral density
PAC	Plasma arc curing light
PNG	Portable Network Graphics
PSA	Prostate specific antigen
QTH	Quartz-Tungsten-Halogen
TIFF	Tag image file format

TIFF-EP Tag image file format-Electronic photography

Acknowledgements

I gratefully acknowledge my supervisor Dr. Dirk Arnold for his guidance, encouragement, support and patience throughout the duration of my MCS program.

I would like to thank Bryan Thomas D'silva and the team at Bluelight Analytics Inc. - Alex Hurley, Chris Felix and Derek Leblanc for their help, insights and resources.

Chapter 1

INTRODUCTION

This chapter will first give an introduction about dental curing light in Section 1.1 including the curing process and different types of LCU and their characteristics. Then Section 1.2 will explain the degradation problem in the dental practice, the consequences, the existing methods in measuring the irradiance of the LCUs and the difficulties in the measuring. Section 1.3 introduces a proposed solution based on cell phone camera technology and its relationship with this thesis. The use of cell phone technology was proposed by Bluelight Analytics Inc., a Halifax based company that develops technologies that help improve light curing outcomes in dentistry. An Android implementation of a cell phone based system for measuring the output of LCUs was created by Bryan D'Silva in the context of a Masters project[2]. The purpose of this thesis is to thoroughly evaluate the accuracy that can be achieved using that system. Last, Section 1.4 gives an overview of this thesis.

1.1 Dental Curing Lights

Fillings and repairs are common dental procedures in the dentists daily work. When the patients need treatment on their teeth that have decay, cavities or fractures, dentists will repair such teeth by putting curable materials in them. In polymer chemistry and process engineering, curing is a term that refers to the toughening or hardening of a polymer material. [1]

According to Mangat et al.[8], the first light-curing resin composites were introduced in the early 1960s which were adapted in dentistry as restorative/filling materials or adhesives. Neumann et al.[9] state that photoinitiators are the chemicals utilized in dental materials that launch the curing process upon absorbing light. The dental light curing unit (in this thesis, this term or LCU is used interchangeably with 'dental curing light' or 'curing light') is a handheld device with a light source

[1] https://en.wikipedia.org/wiki/Curing_(chemistry)

and a guide that transmits the light to a tip. It is placed directly over the tooth that has the material in it and turned on to emit light of a spectrum range appropriate for curing the material for several seconds until the material is cured. Different photoinitiators may absorb light in different spectrum range and the curing efficiencies depend on to what extent the wavelength of the irradiated light overlaps with the absorption spectrum range.

Since the first dental curing light introduced in the 1970s, different types of light sources have been used in the LCU, e.g. Quartz-Tungsten-Halogen (QTH), plasma arc curing light (PAC), Laser and light emitting diodes (LED).

The first dental curing light - Nuva Light, used ultraviolet light (about 365nm) to cure the material relying on the benzoin ether-type compounds photoinitiator.[8] The UV curing lights were not very effective due to the wavelengths shorter than the absorption spectrum range of the photoinitiator limiting the depth of cure. And the short wavelength's energy being exposed to human eyes could have potential risks, they have been replaced by the visible light curing unit.

Curing of dental composites with blue light ($410nm - 500nm$) was introduced in the 1970s. Light in this spectrum range is the most effectively absorbed by the photoinitiator camphorquinone (CQ).[8]

- Rueggeberg[14] presents that QTH curing light produces the blue with a QTH bulb combined with a filter. Because of the high temperatures that the filament generates, the QTH curing unit had to be fan-cooled in order to extend the working time of the source and allow the halogen cycle to operate correctly. Due to Halogen bulbs have a limited effective lifetime of around 50 hours, frequent monitoring and replacement of the curing light bulb is required.

- The PAC was introduced using a high-intensity light source for faster curing. The manufacturer claimed that 3 seconds of PAC irradiation would achieve similar material properties compared to 40 seconds curing with the QTH curing unit. However, to perform adequately clinically, multiple 3-seconds exposures were typically required.[8] These units had to be highly filtered, as they generated large amounts of infra-red light (resulting in heat generation at the target) as well as ultraviolet (having dangerous ozone formation potential).[14]

- Argon lasers emit blue-green light of activated argon ions in selected wavelengths (between 450 and 500 nm). Compared with conventional visible light curing, lasers produce little heat, because of limited infra-red output. It uses fiber optic cable whose radiant output allows shorter curing time than QTH. A major limitation of arc and laser lamps is that they have a narrow light guide (or spot size). This requires the clinician to overlap curing cycles if the restoration area is larger than the curing light.[14]

- LED dental curing light was first introduced to the commercial market at the end of year 2000. The spectrum flux of LED is concentrated over a much narrower bandwidth than that of QTH or PAC and thus requires no filters to produce blue light. LED convert electricity into light more efficiently, thereby reducing heat generation to the extent that cooling fans may not be required or need only be of low capacity. The LED has lifetimes of over 10,000 hours thus no need to replace the light source frequently. Because of LED's characteristics, the LED dental curing light is more cost-effective than QTH and PAC. During the last few years, three generations of LED curing light have been developed. A typical design of the first generation LED curing lights used an array of multiple, individual single-emitting chips (each chip providing 30–60mW) as the light source to emit blue light of wavelength 450nm–470nm which is limited to the dental material with photoinitiator CQ. The second generation of LED curing lights adopted more powerful LED chips to shorten the exposure time. The third generation of LED curing lights utilized blue LED chips together with low power UV LED chips to provide wavelengths that are effective for not only CQ but for the alternative set of initiators as well, creating the equivalent of a "broadband LED" curing light.[14] Compared to other types of energy sources, LED curing lights are cost-effective, lightweight, can be battery powered for portability and more efficient, thus widely adopted in dental clinics.

The irradiance is the radiant power received by the material surface per unit time per unit area. The radiant exposure (J/cm^2) is calculated by multiplying the irradiance by the time duration for irradiation.[13] Krämer et al.[7] study the light curing of resin-based composites used in LED and report that the same degree of resin-based composites conversion is produced by a fixed amount of radiant exposure,

leading to the recommendation of 21-24 J/cm^2 for proper polymerization of a $2mm$ increment of resin-based composites. So the curing depth depends on the irradiance received by the material and the time the material exposed to the light.

1.2 Problems In Dental Practice

As explained in Section 1.1, for a certain curing light and certain restorative materials, the irradiance received by the materials determines the time it needs the light on for the material to cure. A dental light curing unit manufacturer may provide suggestions on the ideal light exposure time, however, the radiant exitance degrades over the lifespan of the light curing unit. According to BlueLight Analytics Inc.'s research, deterioration of curing light output can be affected by several factors including light quality, maintenance and frequency of use. Some lights may start deteriorating upon first use while others may remain consistent for many years (5-10 years). The extent of deterioration can be as high as 99% drop in intensity and not be visibly detectable because the light is very damaging to the eyes. Lights can also have manufacturing defects or be dropped and damaged affecting it's output. A drop in 10% might not be significant on curing times required for materials but a drop of greater than 50% would certainly have a significant impact. Every material has an energy requirement and instructions for use to guide curing times but also most have a minimum stated intensity required. As an example, a common minimum output is $400mW/cm^2$ so when the light output is less then it doesn't matter how much time is used, the intensity is not sufficient and the light would have to be replaced to satisfy the material requirement. Thus the curing times need to be updated reflecting the change in irradiance to avoid an under-curing or over-curing process. If dentists pick the curing time inappropriate for the actual irradiance, too little or too much energy could be delivered to the resin-based composite materials. Under-cured resins are a significant cause of restoration failure due to fracture, secondary caries, or excessive wear of the restoration. Additionally, Shortall et al.[13] analyze the issues in light curing and indicate that when dental resin-based composite materials are not optimally cured (and thus do not reach a sufficient degree of monomer conversion), they are more likely to leach toxic substances. On the other hand, light curing delivers energy that causes a temperature increase in the tooth and surrounding oral

tissues. Shortall et al.[13] also indicate that arbitrarily increasing exposure times in an effort to prevent under-curing may damage the pulp and surrounding tissues.

Measuring irradiance is a challenging task. The radiant exitance from a dental light curing unit is the radiant power emitted by a light source per unit time per unit area. While irradiance is the radiant power received by a surface per unit time per unit area. Although both quantities have the same units: mW/cm^2, they can only be considered to be numerically equal when the distance between the emitted light and the target material is zero. Shortall et al.[16] provide an overview of robust spectrometer-based methods for characterizing radiant exitance of dental LED light curing units and indicate that at non-zero distances, the irradiance from most LED devices attenuates with target distance as the light spreads out over a wider area. As Shortall et al.[16] present, the following challenges exist: the diameter of the LCU optic or exit window may range from $< 5mm$ to $> 10mm$ and there may be non-uniformity of the light beam-profile; the target surface area (diameter) will vary with different clinical scenarios or laboratory test setup requirements; the LCU optic – "target" distance can vary in clinical practice; LED-LCUs may incorporate one or more LED-chips each outputting a different wavelength range; the irradiation time can vary from $1s$ to $20s$ or more; power output varies over time with pulsed or modulated cure protocols.

Rueggeberg[14] reviews dental light curing technologies and indicates that integrating sphere light collection devices coupled to spectro-radiometers are considered as the gold standard for the optical characterization of dental LCUs in the laboratory. However, laboratory grade spectrometers are not cheap and not portable.

Handheld dental radiometers are used in clinics for measuring the output of light curing units. They usually contain silicon photodiodes that convert light into electric current, then an analog or digital meter displays the output from the curing light. However, there are concerns regarding their accuracy. Price et al.[12] compare four brands of dental radiometers, three sample radiometers from each brand and conclude that each brand as a group was not within twenty percent of laboratory grade spectrometers. They present that the type of curing light measured had a significant effect on the accuracy of the radiometer. There was significant variability of the irradiance readings between radiometer brands, and between irradiance values

recorded by the three samples of each brand studied.

CheckMARC by Bluelight Analytics Inc. is a portable spectrometer based instrument featuring a $16mm$ diameter active light collection area with a Teflon diffuser window to measure the irradiance of light curing units and suggests curing times accordingly (Figure 1.1). The measurement is taken with a zero source-to-sensor distance and allows any currently available light curing unit tip size. Shortall et. al.[16] validated on eight LED light curing units and concluded that the results of the measurements made by the CheckMARC device are within two percentage points of measurements made by the Integrated Sphere Spectrometer with the exception for one light curing unit which differed by about ten percentage points because of the convex nature of the surface of its tip. Bluelight Analytics have since traced the lower accuracy to inter-reflections of light between the light tip and the surface of the measuring device and have been able to resolve the issue in software. The current system measures the output with an accuracy close to a laboratory grade spectrometer. However, due to the cost of the equipment and requirement of trained professionals, it is not practical for every dental practice to buy the equipment. Even though Bluelight Analytics Inc. provides a service to dental practices to make routine measurements by trained professionals, frequent measurements are not usually possible. Between two measurements, LCUs' light output can deteriorate significantly and curing with inadequate time would result in restoration failures.

Figure 1.1: CheckMARC by Bluelight Analytics Inc.[2]

1.3 Proposed Solution

In order to let dental practice monitor the intensity degradation effectively, Bluelight Analytics Inc. proposed using a cell phone camera to measure the output of the light curing unit to complement the CheckMARC service. It is low in cost and easy

to use by dentists themselves. D'silva and the Bluelight Analytics Inc.[2] reviewed the components of a dental spectrometer and implemented a proof of concept of the proposed solution including the hardware setup on a cell phone camera and the software based on Android system.

Using cell phone cameras to capture images of LCU light source is a challenging task. The LCUs emit light of high intensity that could damage the camera sensor. Each time the light turned on, it can only last for seconds, pressing the camera shutter too early or too late could miss the time window. Photographed images generally exhibit a radial falloff of intensity as we move away from the center of the image, which is called vignetting. So if the light is captured towards the edge of the image, the pixel intensities are less than they should be. The distance between the light and the camera is another factor that could impact the image pixel intensities. The larger the distance is, the dimmer the light pixels are. The angle between the LCU light guide tip and the camera could also affect the pixel intensities in the image especially for some LCUs that have a spherical guide tip instead of a flat one. D'silva[2] introduces a filter stack attached to the cell phone camera and an auto-capture algorithm to control the capturing condition which will be covered in Section 2.3. With this hardware and software implementation, D'silva captures JPG images and tests the effect of estimating the LCU power by using these images.

Our set-up differs from that of D'silva in two aspects:

- Burst mode: D'silva's test was based on the camera capturing a single image at a time. If the capturing is triggered when the light is at an imperfect position or an imperfect moment, it may impact the accuracy of the estimation(details are covered in Section 3.3). The camera burst mode setting allows us to capture a sequence of images with very short time intervals instead of a single image thus reduce the risk of using the imperfect images in further calculation. So in this thesis, image sets captured with camera burst setting will be used in the analysis.

- Raw images and the impact of using JPG: The raw image format (DNG format) records the pixel values linearly to the light irradiance received by the image sensor but the JPG format pixel values are not linear to the light irradiance. So the non-linear JPG pixel values do not reflect the real light intensity received

by the camera sensor which may result in inaccurate estimation of the light power. D'silva estimates the light power with JPG format. This thesis will do the analysis based on DNG format. With gamma decoding applied to the images of JPG format, JPG images could achieve approximate linear to its DNG counterpart. The analysis based on the JPG images applied gamma decoding will also be covered in this thesis.

Our analysis is also distinguished by comparing the accuracy between DNG format and JPG format in different aspects including different exposure times, different image sizes, different intensity thresholds for foreground/background separation.

1.4 Thesis Coverage

The remaining chapters are organized as follows: Chapter 2 gives an overview of the cell phone camera image capturing technology, storage formats, application besides ordinary photography and introduces D'silva's implementation of the proposed system. Chapter 3 introduces image processing and accuracy calculation methods. Chapter 4 applies the methods on the image sets taken for different curing lights, uses the readings of CheckMARC by Bluelight Analytics Inc. measuring these curing lights as the baseline and calculates the relative error and overall variation on different aspects and verify the accuracy by applying the methods on the image sets used in [2]. Chapter 5 remarks the conclusion and future work.

Chapter 2

BACKGROUND

This chapter introduces the core technology of the cell phone camera hardware, the development of the camera phone and the camera phone's application in the scientific research in Section 2.1. Cell phone images can be stored in the raw format and the processed format. Section 2.2 introduces the most commonly used raw format - DNG and the processed format - JPEG. Both are used for the analysis in the later chapters. Section 2.3 introduces the hardware setup and the auto-capture algorithm implemented by D'silva to capture the LCU's light by cell phone camera.

2.1 Camera Phone Development And Application

The core technology of any digital camera is the image sensor, the lens, and its image-processing software. Phone manufacturers can opt for one of two major image sensor technologies: charge-coupled devices (CCDs) and complementary metal oxide semiconductors (CMOS). Nearly all camera phones use CMOS image sensors, due to largely reduced power consumption compared to CCD type cameras. Having been continuously improved over years, modern CMOS sensors become equal or superior to CCDs in terms of image quality, image speed, and more suitable for mobile phone built-in camera.[2][10] With the pixel size scaling down, the amounts of pixels on an image sensor continually increased, thus providing a higher image resolution. In the meantime of developing the image sensor, camera phone lenses are also been improved.

Since the first camera phone came into the market in the late 1990s and early 2000s, the technology of the camera phone has been developed rapidly in both the hardware and software. During the 2010s, the image sensor increased the resolution from 0.11-megapixel to 16-megapixel, white balance control, self-timer, digital zoom, auto-focus, image stabilization had been added, the flash had been developed from

[2]https://en.wikipedia.org/wiki/Image_sensor

basic flash to LED flash to the Xenon flash. Multi-shot option for taking eight quick photos in a row was added in 2004. Since Apple Inc. announced the first iPhone in 2007, mobile applications for smartphones have grown rapidly during the next 10 years. iOS and Android system have been dominating the mobile market and the Android has obtained 72 percent of the market share by March 2020.[3] It provides APIs to control the camera and allows users to develop their own image processing functions. Android version 5.0 (Lollipop) released in 2014 introduced camera2 API which gives control over parameters like the exposure time and the ISO sensitivity and supports storing images in the DNG format.

With the camera phone technologies being continuously improved and the need for low-cost, portable analytic devices, camera phone have been proposed as tools for solving measurement problems in a wide range of areas:

- In analytical chemistry, smartphone-based spectrometers in both absorption and emission modes have been designed and improved to determine Fe2+ in medicine samples and Na+ in saline solution and natural water samples[11].

- With attached components, a cell phone has been turned into a 350× microscope which is capable of transmission and polarized microscopy modes and is shown to have 1.5-micron resolution and a usable field-of-view of about $150 \times 150mm$ with no image processing, and approximately $350 \times 350mm$ when post-processing is applied. Smith et al.[17] image both stained and unstained blood-smears showing the ability to acquire images of similar quality to commercial microscope platforms.

- Barbosa et al.[1] introduce a portable smartphone quantitation of prostate specific antigen (PSA) in a fluoropolymer microfluidic device. The smartphone-based colorimetric detection system not only offers methods as such to healthcare applications but also used to estimate the age of the bloodstain in forensic analysis[15, 6].

- Ghuzlan et al.[3] introduced computer-vision cellular-phone-based methodology and scheme to determine the shape properties (Flatness Index, Elongation Index, and Roundness Index) of coarse aggregate particles for asphalt mixtures.

[3]https://gs.statcounter.com/os-market-share/mobile/worldwide

- Whiteson et al.[19] propose an approach for searching for ultra-high energy cosmic rays with the cell phone camera. Extensive air showers generated by cosmic rays produce muons and high-energy photons, which can be detected by the CMOS sensors of cell phone cameras. The small size and low efficiency of each sensor are compensated by the large number of active phones. They show that if user adoption targets are met, such a network will have significant observing power at the highest energies.

In all cases, the low cost and wide availability of cell phone camera technology offer advantages that at least partially compensate for any technical shortcomings of the dedicated equipment.

2.2 Cell Phone Image Format

Digital cameras record images by using an array of photosites to collect photons striking them which are then transformed to electrical signals and the strength of the electrical signals are measured and quantified as digital values of each pixel. Since the photosites cannot distinguish colors, pixel values can only be saved as a scalar value without color information. To capture color images, Color Filter Array (CFA) that permits only particular wavelengths of light is placed over each photosite. In this way, each pixel carries information about a single color channel: red, green, or blue. Figure 2.1 illustrates the most common CFA - Bayer array which contains twice as many greens as red or blue because the human eye is more sensitive to variation in shades of green and it is more closely correlated with the perception of light intensity of a scene.

Such an image collected directly from the camera sensor is called the raw image.

DNG (Digital Negative) is a standard non-propriety format introduced by Adobe in 2004 to store the raw image. Before DNG, different digital camera manufacturer has its own raw image formats. The lack of a standard format for camera raw files creates additional work for camera manufacturers because they need to develop proprietary formats along with the software to process them. To address such issues, Adobe introduced the DNG format. An image stored in the DNG format is self-contained, providing specific information about the camera and the settings under which the image is captured. This allows for a greater degree of control and flexibility

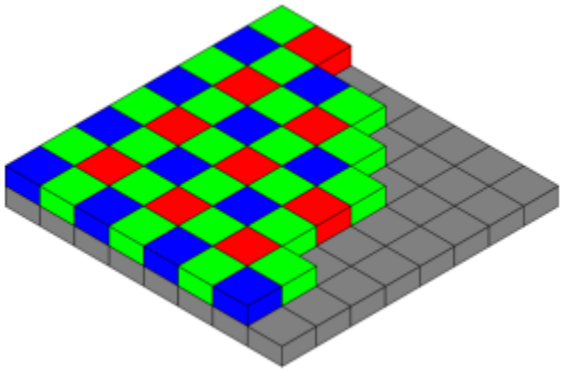

Figure 2.1: Bayer CFA image taken from [4]

over the image. This is useful for work with professional photography, data archival and computational photography.[5] DNG is an extension of the TIFF 6.0 format and is compatible with the TIFF-EP standard, which declares and describe their content by means of tags in the header and in Image File Directories (IFDs) within the file. Figure 2.2 is an example of the tags read from a DNG file:

```
        ExposureTime: 0.0667
              FNumber: 2
     ISOSpeedRatings: 80
    DateTimeOriginal: '1970:02:17 21:08:17'
         FocalLength: 4.6700
          DNGVersion: [1 4 0 0]
  DNGBackwardVersion: [1 1 0 0]
   UniqueCameraModel: 'Nexus 5X-LGE-google'
       CFAPlaneColor: [0 1 2]
           CFALayout: 1
 BlackLevelRepeatDim: [2 2]
          BlackLevel: [52 52 52 52]
          WhiteLevel: 1023
        DefaultScale: [1 1]
   DefaultCropOrigin: [8 8]
     DefaultCropSize: [4016 3008]
```

Figure 2.2: Partial DNG Metadata.

Due to the size of the camera raw image is large and it must be processed before they can be used, typically through software proprietary to the camera manufacturer.

[4]Colin M.L. Burnett., A Bayer pattern on a sensor in isometric perspective/projection, https://en.wikipedia.org/wiki/User:Cburnett#/media/File:Bayer_pattern_on_sensor.svg, CC BY-SA 3.0, no changes were made upon it.

[5]https://www.adobe.com/content/dam/acom/en/products/photoshop/pdfs/dng_spec_1.4.0.0.pdf

Before the DNG format being introduced, it was not the raw image but a processed format JPG (Joint Photographic Experts Group) that supported by the first camera phone. And although more other image formats are now supported by cell phone platforms, JPG is still the most commonly used smart phone default image format which is more compatible across different platforms.

JPG was created in the early 1990s defining a general-purpose compression standard to reduce image size, allowing more efficient storage and transmission. JPG provides a standard for photographic images enabling interoperability between different manufacturers. Although a JPG file can be encoded in various ways, most commonly it is done using a baseline sequential codec outlined in [18]. The compression method is usually lossy, meaning that some original image information is lost and cannot be restored. There is an optional lossless mode defined in the JPG standard, however, which is not widely supported in products. JPG format uses 24-bit depth (8bit per RGB color channel) for storing each pixel.

Digital cameras record light using electronic sensors that usually respond linearly, when doing color space transformation to convert the linear raw data to RGB JPG format, Gamma encoding is usually performed for displaying purpose. The Gamma (Power-law) transformations have the basic form $s = cr^{\gamma}$.[5] Plots of s versus r for various values of γ are shown in Figure 2.3.

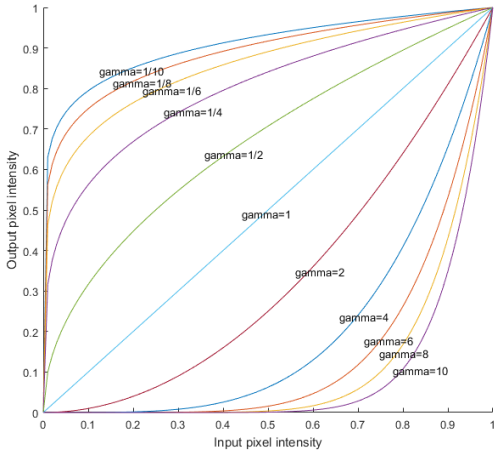

Figure 2.3: Gamma transformation.

PNG (Portable Network Graphics) is another format that widely adopted in cell

phone applications. However, it is normally used for saving screen shots instead of saving photos. PNG was introduced as an patent-free replacement for GIF (Graphics Interchange Format). PNG supports 24-bits RGB color as JPG does, with an optional alpha channel, it can also support transparent color. PNG also supports lossless compression but for photographic images which is typically dominated by soft, low-contrast transitions, and an amount of noise or silimar irregular structures, using PNG instead of a high-quality JPEG would result in larger file size with negligible gain in quality. On the contrary, for the images containing sharp transitions and large areas of solid color such as text, line art or graphics, the PNG can compress more than JPG can.[6] That is why PNG is normally used for screen shot which usually contains web content while JPG is normally used as default image format of camera captured photos.

The cost of storage and transmission has become much cheaper than before, camera phones have started supporting DNG image formats. Most Android devices supporting the FULL level of functionality for camera2 API support raw SENSOR as an output buffer. DNGCreator class in camera2 API uses the raw SENSOR output buffer to write raw pixel data from the camera sensor to a DNG file. But PNG is not one of the image formats supported by the camera2 API.

2.3 Capturing Images

Working with Bluelight Analytics Inc., D'silva[2] reviewed the components that constitute a dental radiometer and incorporated some into the proposed hardware setup. To avoid high irradiance damaging the camera sensor, they use a setup of stackable neutral density (ND) glass attenuator filters to reduce the irradiance. As shown in Figure 2.4, the setup includes an ND1 and an ND2 filter. The ND1 filter transmits approximately 1/10th while the ND2 transmits about 1/100th of the original intensity. Stacked together, they transmit 1/1000th of the original intensity. The neutral density filter attenuates remove the intensity of all of the visible spectrum wavelengths equally. A Teflon diffuser was added upon the filter stack to make the output of all lights approximately uniform and round. The cost of the filters and the diffuser is about 35$ each, and with a holder, it would be about 100$ in total.

[6] https://en.wikipedia.org/wiki/Portable_Network_Graphics

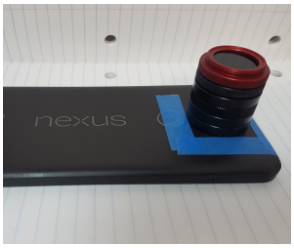

Figure 2.4: Filter Positioning over Android Device.[2]

With the widespread use of Android as a mobile operating system and an introduction of a camera framework allowing control over parameters like the exposure time and provision for uncompressed output formats, D'silva[2] also developed an Android application for auto capturing images in both DNG and JPG formats of the output of the light curing unit.

Capturing an ideal image of the light output from an LCU is a challenging task. It requires the following conditions are all met:

- Zero distance between the tip of the LCU and the filter stack set up on the camera.

  Non-zero distance between the tip and the filter surface will cause the irradiance captured by the camera sensor lower than expected.

- The dental curing light should be kept approximately in the central region of the capture area.

  This is required to mitigate the effect of vignetting. Photographed images generally exhibit a radial falloff of intensity as we move away from the center of the image. Although lens manufacturers attempt to design their lenses so as to minimize the effects of vignetting, it is still present to some degree in all lenses and can be quite severe for some aperture and focal length settings[4]. Goldman found that fixed aperture lenses may transmit thirty percent to forty percent less light toward the edges as compared to the center of the image. Thus, this will potentially lead to a lower than intended irradiance when capturing an image where the light is toward the edges.

- A proper exposure time

An improper exposure time setting will cause over-exposed or under-exposed images.

All these preconditions of capturing an ideal image require a strictly controlled hardware setup, a set of proper camera settings and a careful execution of the process. In the real world, it is not always possible to have the setup and the resources for the ideal conditions. To provide minimum hardware setup and an easy interface to a user to set the required parameters, D'silva developed an auto-capture algorithm including:

- Auto exposure time setting

  Most light sources of LED LCUs emit blue light and a small portion of them emit a combination of blue and ultraviolet light in which the blue light dominates the power output from the LCU. The algorithm extracts the histogram of the blue channel from the image of JPG format (8-bit) and adjust the camera exposure time in the step of 1/5 of the current exposure time until there are no pixels in 255th intensity bin (not overexposed) and there are pixels with intensity larger than 128 (not underexposed).

- Auto capture triggering

  The filter and diffuser setup over the camera sensor blocks out most of the light from the background and makes the light foreground approximately uniform and round. The algorithm defines a threshold of 0.8*(maximum pixel intensity) to separate foreground from the background and defines a 120×120 pixels square in the center of the viewfinder as the bounding box (The JPG resolution is 320×240 pixels set by D'silva[2]. Results reported in Section 4.3 suggest that observations of total intensity are insensitive to image size in a wide range that includes this resolution.). Only when at least 50 percent of the pixels inside the bounding box is made up of foreground pixels, and at least 90 percent of the pixels outside the bounding box are made up of background pixels, the capturing will be triggered. This is to ensure the light approximately in the central region of the image to mitigate the effect of vignetting.

The hardware and software are implemented on Nexus 5X - an Android Smartphone made by LG electronics in collaboration with Google [7]. And all the images of

LCUs using in this thesis are taken with Nexus 5X.

[7]https://www.google.com/intl/en ca/nexus/5x/

Chapter 3

METHODOLOGY

This chapter presents the image processing and analysis methods adopted in this thesis. Section 3.1 introduces the preprocessing steps needed to apply to the DNG image files before they can be used for further analysis; Section 3.2 explains how do we use the total intensity of the pixels forming the light foreground in the image and how do we decide the intensity threshold to separate the foreground and the background pixels; Section 3.3 explains the reason why we use a series of images captured with camera burst mode instead of using single capturing; Section 3.4 uses the first-order moment to determine the center of the light foreground. This will be used in the further analysis to determine a threshold of the distance from the light foreground center to the image frame center to exclude those off-centered images that will have negative impact on the accuracy; Section 3.5 illustrates the DNG-JPG pixel mapping relationship and choose gamma=2.2 to apply gamma decoding to the JPG images; Section 3.6 introduces the methods used for measuring the relative accuracy and the overall variation of the images we captured with camera burst mode with the baseline value collected from CheckMARC.

3.1 Image Preprocessing

DNG is a commonly used format of the raw data from the sensor of the camera that contains an uncompressed image as well as a set of meta-information. The nature of the raw data is that it is a single channel intensity image, possibly with a non-zero minimum value to represent 'black' and a maximum value (typically 10-14 bits integer) to represent the saturation point of the raw sample data. The size of the raw image may also be larger than the expected pixel dimensions of the camera, including a border of unexposed pixels. Thus the raw images must be processed before they can be used for analysis. Following are the steps of the preprocessing according to the meta-information stored in DNG tags:

- Crop to Active Area

  Most camera sensors measure the zero light (a.k.a. thermal black or black current) encoding level using fully-masked pixels at the edges of the sensor. The active area is the rectangle defines the active (non-masked) pixels of the sensor. The DNG tag ActiveArea contains four short or long integers specifying the top, left, bottom, right coordinates of the active area rectangle. Cropping to the active area is to exclude those masked pixels out of this rectangle.

- Extract Blue Channel

  The values of DNG's metadata tag PhotometricInterpretation,CFALayout, CFA-Pattern and CFARepeatPatternDim, indicate that the Nexus 5X uses Bayer CFA of Rectangular (or square) layout (Figure 2.1). The origin of the repeating CFA pattern is the top-left corner of the ActiveArea rectangle and the repeating pattern is 'RGGB' for each 2*2 pixel cluster. Since most of the LED curing lights emit blue light, only a few emit light of blue and ultraviolet combination and the blue light dominates the output power, only the blue channel pixels are extracted for further analysis.

- Black Subtraction

  The black encoding level information extracted from the masked pixels is specified by the DNG tag BlackLevel as a repeating pattern. The origin of this pattern is the top-left corner of the ActiveArea rectangle. Black subtraction is to subtract the value of the DNG tag BlackLevel (If the value of Black-LevelDeltaH and BlackLevelDeltaV are not empty which is not the case of the DNG files used in this thesis, then subtract the sum of the black levels specified by the BlackLevel, BlackLevelDeltaH, and BlackLevelDeltaV) from each pixel.

- Crop to the Final Area

  Raw images often store extra pixels around the edges of the final image. These extra pixels help prevent interpolation artifacts near the edges of the final image. Tag DefaultCropOrigin specifies the origin of the final image area, in raw image coordinates, relative to the top-left corner of the ActiveArea rectangle. Crop to final area is to exclude those extra edge pixels.

3.2 Measure The Light Power

The WhiteLevel tag in the DNG images indicates the saturated encoding level for the raw sample values. DNG images captured by Nexus 5X has the WhiteLevel value of 1023. By subtracting the BlackLevel 52 (as described in Section 3.1, the BlackLevel represent the zero-light encoding level and needs to be subtracted from the pixels in ActiveArea), the possible maximum pixel value is 971. Figure 3.1 is a preprocessed DNG image of a capturing with $1/30s$ exposure time for the LCU D1 high power mode and its logarithmic histogram. From which we can see the amount of the pixels near-zero intensity is large.

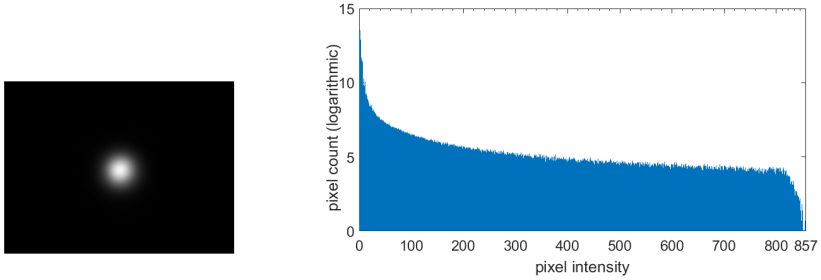

(a) preprocessed DNG image

(b) preprocessed DNG histogram

Figure 3.1: logarithmic histogram of pixel count for each intensity.

The light power estimation should exclude those background pixels and based on the total intensity of only the light foreground in the image. To determine the curing light foreground area in the image, a percentage of the maximum intensity value of each image is used as a threshold and only the pixels' intensity value greater than the threshold is considered within the light area. The pixels outside the light area will be considered as background and their values are treated as noise and will not be involved in the further calculation. Figure 3.2 uses three DNG images captured for the curing light D1 Standard mode with different exposure time to illustrate the total intensity (summed intensity of the pixels) of the foreground and background of different threshold ranging from 1% to 30% of the maximum intensity. The total intensity of the background pixels can become larger than the total intensity of the foreground pixels as the threshold increase, especially for the image captured with

shorter exposure time.

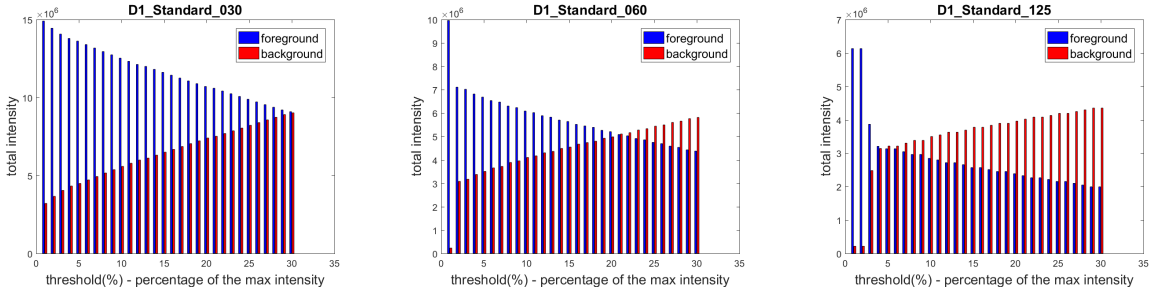

(a) $1/30s$ exposure time (b) $1/60s$ exposure time (c) $1/125s$ exposure time

Figure 3.2: Total intensity of DNG format capturing with different exposure time for the LCU D1 Standard Mode against different threshold.

Figure 3.3 compares three thresholds (1%, 5% and 30%) for the same three images as Figure 3.2 and illustrates the thresholds in the light image and the graph of the intersection through the light's center below the image. The green, red and magenta colors in the image mark the boundaries (coloring the first and the last pixels that equal to the threshold intensity when scanning each row of pixels from left to right) determined by 1%, 5% and 30% thresholds separately, which are also illustrated at the both sides of the intersection as the vertical lines in the corresponding colors. For images captured with longer exposure time ($1/30s$ and $1/60s$), the green vertical line (1% threshold) is closest to the edge position on the intersection curve. But when the exposure time decrease to $1/125s$, the 1% threshold cannot distinguish the edge from the background. Compare with the red (5% threshold) and the magenta (30% threshold) vertical lines, the 5% threshold is closer to the edge position of the intersection curve, so the 5% of the maximum intensity is used at first as the threshold above which to calculate the pixels' total intensity. (Chapter 4.4 will do further analysis about the different intensity thresholds.)

3.3 Burst Image Sets

Due to the following reasons, a single capturing of the curing light may not be good enough for estimating the light power and result in low accuracy.

- Captured at an imperfect position - As described in Section 1.3, to prevent the

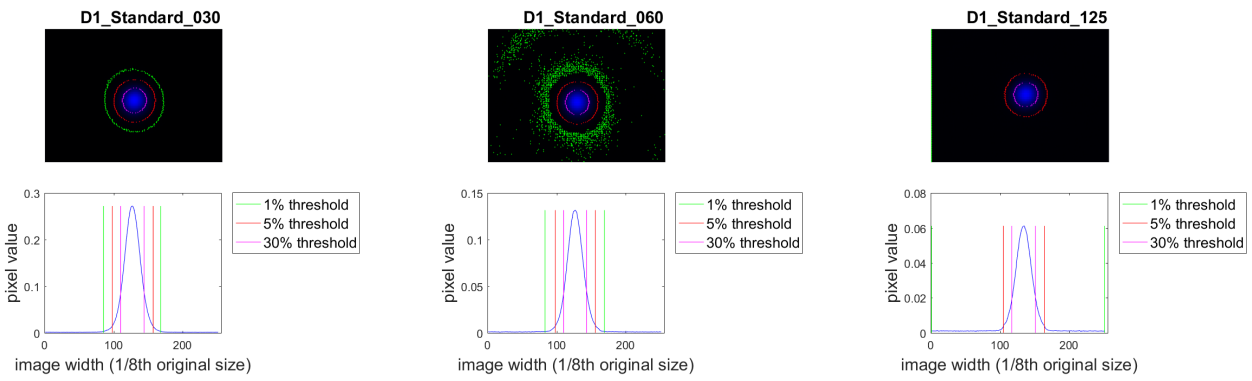

(a) 1/30s exposure time (b) 1/60s exposure time (c) 1/125s exposure time

Figure 3.3: Light foreground edge thresholds upon intersection through light center of images.

intense light from the curing light damaging the camera sensor, we use a stack of neutral density filters and a Teflon diffuser attached to the cell phone camera when taking images. The diameter of the filters is larger than the camera sensor and the light tips, so even with the auto-capture algorithm, the light still can be captured off the image center. Due to the vignetting effect as described in Section 2.3, when captured off the center of the image, the pixels intensity of the light foreground drop off than it is captured at the center of the image. Figure 3.4 compares an image with the light at the center position (Figure 3.4a) and an image with the light off-centered position (Figure 3.4b). with the method described in Section 3.2 of measuring the light power by summing the pixel intensity values above a threshold, Figure 3.4c shows that the total intensity above 5% of the maximum intensity for the DNG format of Figure 3.4b is 13% less than that of Figure 3.4a. Re-centering the off-centered image cannot correct the pixel intensity value and due to we lack the information of the physical parameters of the lens, to apply a vignetting correction on those off-centered images is difficult.

- Captured at an imperfect moment - The curing lights we used to capture images can last for 2 to 20 seconds for different modes and normally shorter for higher

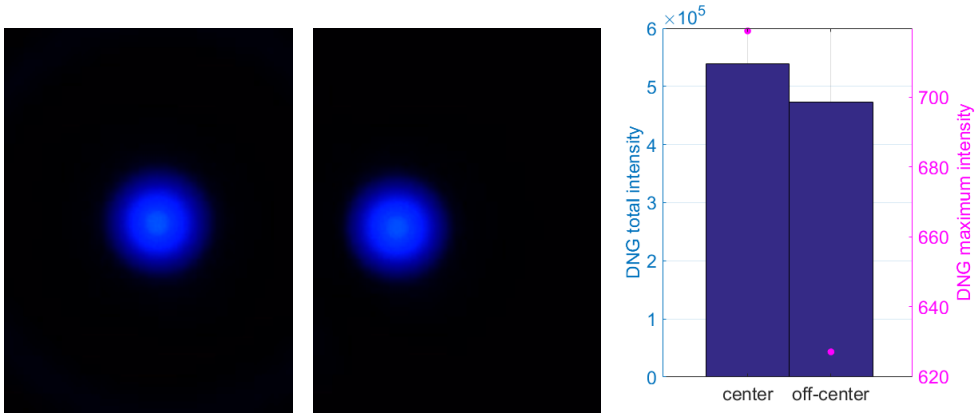

(a) center (b) off-center (c) total intensity difference

Figure 3.4: Single image center vs. off center.

mode. To capture a single image right on time is challenging. An image may be captured at the beginning moment when the light turned on or the end moment when the light turned off. At such a moment, the light may not emit with full power thus causing the image total intensity less than expected. It is also possible that the exposure time only partially overlaps with the time that the light is on, resulting in the image total intensity less than expected. Figure 3.5 shows three images taken sequentially at the time interval of about 970ms for the CybirdXD curing light high mode. The light cannot last longer for us to take the fourth image. In terms of the total intensity above 5% of the maximum intensity, the 1st image is 5% less than the 2nd image; and the third image is 1% less than the 2nd one.

Turning on the burst mode of the cell phone camera to take a sequence of images with a short time interval (the time interval differs from one cell phone to another and depends on the time to automatically post process each image by the cell phone, e.g. encoding JPG from the raw image) allows us to select those proper ones for the light power estimation. In this thesis, an image set refers to a set of sequential images captured by one shutter clicking with the camera burst mode setting.

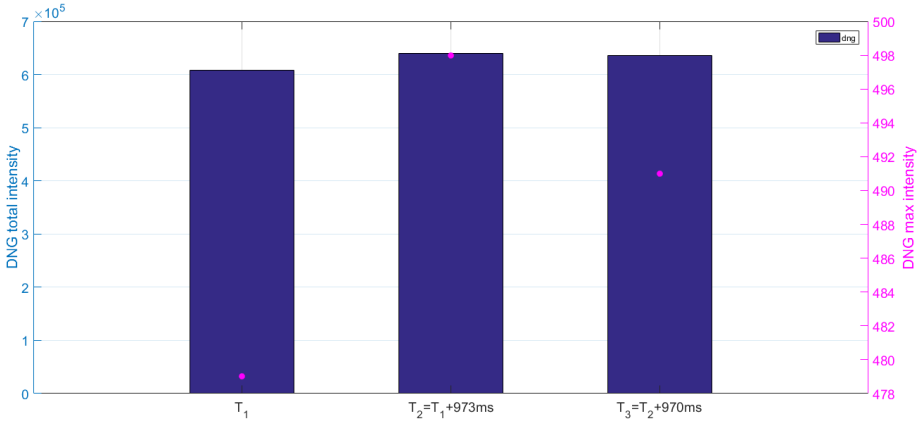

Figure 3.5: Single image imperfect time.

3.4 Light Center Determination

Since the light captured off the center can result in less total image intensity than those captured at the center as shown in Section 3.3, the distance of the light center from the image frame center need to be measured for each image to determine a threshold above which an image should be excluded from degradation estimation. The method used to determine the light center is described in this subsection.

Since the curing light tips end are of round shape and the images are captured with a diffuser, the light in the image is a spot in round shape and the closer to the center the higher the pixel intensity is. Thus the light center can be estimated by the center of mass of the image. The coordinate of the center of mass is calculated from the first-order moment as

$$C_x = \frac{M_{10}}{M_{00}} = \frac{\sum_{x=1}^{w}\sum_{y=1}^{h} xI(x,y)}{\sum_{x=1}^{w}\sum_{y=1}^{h} I(x,y)}$$

$$C_y = \frac{M_{01}}{M_{00}} = \frac{\sum_{x=1}^{w}\sum_{y=1}^{h} yI(x,y)}{\sum_{x=1}^{w}\sum_{y=1}^{h} I(x,y)} \tag{3.1}$$

where

(C_x, C_y) is the coordinate of the light center

M_{00} is the zeroth-order moment

M_{10} and M_{01} are the first order moments

w and h are the image's width and height

$I(x, y)$ is the pixel intensity value at the (x, y) position

3.5 Gamma Decoding For JPG Format

As described in the Section 2.2, DNG image is linear in response to the camera sensor raw signal. While gamma encoding is performed when the raw data collected from the camera sensor being transformed into JPG format. Figure 3.6a shows the scatter plots of the pixel value of JPG format against the pixel value of DNG format (resize to the JPG size) from an image set including thirteen images of both DNG and JPG formats captured with burst mode for a curing light with exposure time $1/30s$ (that are properly exposed and light's foreground is located at the center of the image). It shows nonlinear relationship and a narrow range of dark DNG values being mapped into a wider range of JPG values. So applying gamma decoding on the JPG format can adjust the JPG pixel values and the scatter plot becomes approximately linear as Figure 3.6b when $\gamma = 2.2$ though it is not perfect, especially for the darker pixels.

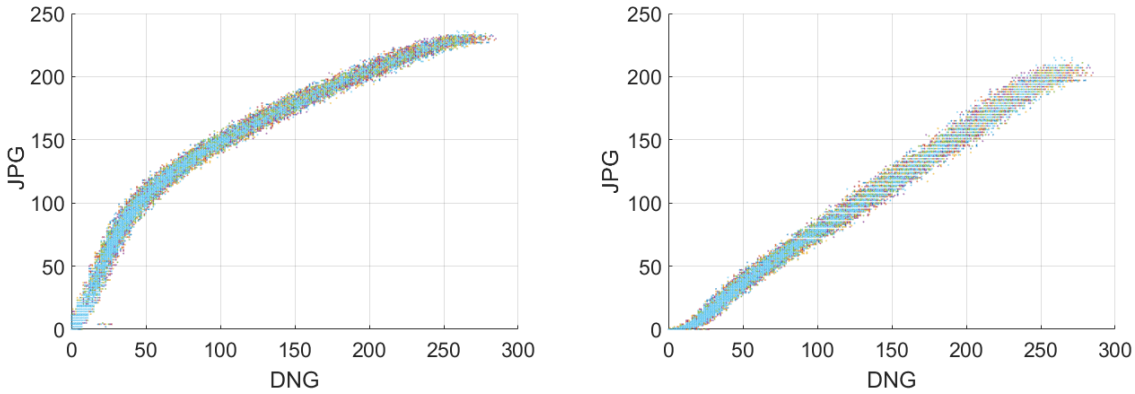

(a) Without gamma decoding

(b) gamma=2.2

Figure 3.6: Scatter plot of a burst image set for a curing light in standard mode.

3.6 Accuracy Measurement

As discussed in Section 1.2, BlueLight's CheckMARC device can provide an irradiance measurement that we consider accurate for the purpose of this thesis. So this thesis uses the CheckMARC readings as the baseline to evaluate the accuracy of the intensity measurements based on cell phone camera images. The CheckMARC measures irradiance in the unit mW/cm^2, but from the image captured by the cell phone camera based device described in Section 1.3, we can only get pixel intensities but lack of tools to transform it to the corresponding irradiance values. Therefore it is not feasible to measure its absolute accuracy, but the relative accuracy is measurable by calculating the relative error - ratio of the total pixel intensity of images taken for different power modes of an LCU and comparing it to the ratio of the CheckMARC readings for these power modes.

For each power mode of an LCU, we will use the burst camera setting to capture two to three image sets (each image set contains the images taken in one burst sequence) for each exposure time setting. The relative error is calculated in the following steps:

- First, collect all the image sets for one curing light and calculate the total intensity (the sum of the foreground pixels' intensity value divided by the exposure time) of each image;

- Second, select the median value from each image set and group them by the light mode. (E.g. If we have image set1 taken for the high power mode, and set2, set3 taken for the low power mode. We select median value from set1, set2, set3 as m1, m2, m3. Then put the m1 into group1, and put m2, m3 into group2);

- Third, for each selected image in one light mode group, cross pair with each selected image in another light mode group (E.g. the example of the previous step will yield two pairs (m1,m2) and (m1,m3)).

The relative accuracy is inversely related to the relative error calculated as

$$Err = \frac{\sqrt{\frac{\sum_{i=1}^{M}(\frac{X_{i_L}}{X_{i_H}} - \frac{CheckMARC_L}{CheckMARC_H})^2}{M}}}{\frac{CheckMARC_L}{CheckMARC_H}} 100\% \tag{3.2}$$

where

M is the count of the image pairs;

X_{i_L} and X_{i_H} are the total intensity (foreground pixels total intensity divided by the exposure time) of the image for the low mode and the high mode in the ith image pair;

$CheckMARC_L$ and $CheckMARC_H$ are the CheckMARC readings for the low mode and the high mode.

In addition, the variation among all the images captured for an LCU can be measured by calculating the coefficient of variation (CV) for the normalized total intensity across all the images in the image sets captured for different power modes of a curing light. The normalized total intensity is the sum of the foreground pixels' intensity value divided by the exposure time and the CheckMARC reading. This normalized total intensity makes image sets comparable even when they are captured with different exposure time and for different light power modes so this thesis uses 'overall variation' to refer to the CV calculated by

$$CV = \frac{\sqrt{\frac{\sum_{i=1}^{N}(Y_i - \frac{\sum_{i=1}^{N} Y_i}{N})^2}{N-1}}}{\frac{\sum_{i=1}^{N} Y_i}{N}} 100\% \tag{3.3}$$

where

Y is the normalized total intensity (the sum of the foreground pixels' intensity value divided by the exposure time and the CheckMARC reading) of each image involved;

N is the count of the images involved.

Using CV is because it is suitable when comparing different data sets which have different mean values. Chapter 4 uses image sets captured on a different date and they need to be calculated separately for a possible reason that the capturing condition changed. Thus the CV is more suitable rather than the standard deviation.

Thus the result of estimating the curing light's irradiance with cell phone images is evaluated in two aspects - relative error and overall variation.

Chapter 4

EXPERIMENT AND EVALUATION

Since the curing light degradation occurs during a long period of time, it is not feasible for us to collect images for a certain curing light every several months. But curing lights commonly used nowadays have two to three different power modes, the degradation can be simulated by switching from the high mode to the low mode. The high mode is seen as the light before degradation and the low mode is seen as the light after degradation. So instead of analyzing the images captured months by months, the thesis analyses the images captured for different modes. To evaluate the accuracy of estimating the curing light degradation (simulated by different power modes) from the cell phone images, we captured images of both JPG and DNG formats with Nexus 5X equipped with the filters stack described in Section 2.3. The images are captured with a user holding the tip of the LCU on the surface of the filter setup. We use five different LCUs in total, each having two (high/low) or three (extra high/high/low) power modes. Among them, three LCUs are used in the experiment section. The images are taken on two dates with the camera exposure time setting ranging from 1/250s to 1/8s for 2018-Jan-16 and 1/30s to 1/15s for 2018-Mar-18. Two to three burst image sets are taken without the auto capturing algorithm for each exposure time, each light power mode. Each burst captures nineteen images. Images adopted in the verification section were originally used by D'silva in [2] that contains two further LCUs. These images are not taken with burst mode but with the auto exposure time setting described in Section 2.3. Five image pairs (one image for high light power mode pair one image for low light power mode) are captured for every two modes of each LCU. The verification section will use this set of images to verify if the conclusions made out of the three LCUs used in experiment can also apply to other LCUs and if a more proper exposure time setting could result in better accuracy.

As mentioned in Section 1.3, D'silva [2] implemented the Android based application and tested it with images of JPG format by calculating the relative percentage change from the high mode to the low mode of the five image pairs and chose the median value to compare to the CheckMARC measurement. This thesis mainly focuses on thoroughly evaluating the accuracy that can be achieved using this system. It differs from D'silva's work in that we capture images with camera burst mode; using DNG format and apply gamma decoding on the JPG format and comparing relative error and overall variation on different exposure time, image size and intensity threshold or foreground/background separation.

Excluding imperfect images is described in Section 4.1; The impact of exposure time is investigated in Section 4.2; The impact of image size is studied in Section 4.3; Different foreground/background splitting thresholds are compared in Section 4.4. Section 4.5 uses extra image sets that contain two further LCUs to verify if the conclusions made out of the analysis in the previous sections can also apply to other LCUs.

4.1 Image Selection

Images used for analysis are captured on 2018-Jan-16, 2018-Mar-18, and 2018-Mar-21. The five curing lights involved are D1, CybirdXD, Valo, CybirdGold (8mm tip's diameter), CybirdGold (11mm tip's diameter) and G2 and they are referred to as LCU1 through LCU6. Table 4.1 lists the modes of these curing lights and their irradiance measured by CheckMARC in July 2017. Because the lights were not used in dental practice and activated only infrequently in a lab setting, we assume that no substantial degradation has occurred in the meantime. This is used as the baseline to evaluate the accuracy of the outcome of the images analysis. Images of 2018-Jan-16 and 2018-Mar-18 are captured with burst camera setting for LCU1, LCU2 and LCU3 with the exposure time ranging from $1/250s$ to $1/8s$ (fixed values for other camera parameters). For each exposure time, two to three image sets are captured. Images of 2018-Mar-21 are captured without the burst camera setting for all these five curing lights. Five image pairs are captured for every two modes of each light. The size of the images is set 320×240 pixels for JPG format (This resolution was used by D'silva [2] in his implementation. Results reported in Section 4.3 suggest

Table 4.1: Curing Light Irradiance.

Light	**Mode**	**Irradiance (mW/cm^2) (CheckMARC readings)**
LCU1	High	2445
	Standard	791
LCU2	High	2445
	Standard	1332
LCU3	Extra	2100
	High	1290
	Standard	920
LCU4	High	1438
	Low	786
LCU5	High	1170
	Low	778
LCU6	High	2333
	Low	1313

that observations of total intensity are insensitive to image size in a wide range that includes this resolution.) and 3028×4080 pixels for DNG format.

Not all images captured on 2018-Jan-16, 2018-Mar-18, and 2018-Mar-21 are suitable for estimating light power. Some are captured out of the period the light turned on; some are with the light off-center position; some are overexposed or underexposed. These images cannot reflect the real power of the light and need to be filtered out before further analysis.

Figure 4.1 is the bar graph of the total intensity of each image in all the burst image sets captured for the LCU1, LCU2, and LCU3 on 2018-Jan-16 and 2018-Mar-18. The total intensity is a summation of the intensity of the pixels that form the light foreground determined by the threshold 5% of the maximum intensity. For each LCU there are three sub-graphs: the total intensity of the DNG format (resized to the same size of the JPG format -320×240 - with nearest-neighbor interpolation), the total intensity of the JPG format applied gamma decoding and the distance of the light center away from the image center of each JPG image. The sets are named as "LightId_Date_ExposureTime_FolderName".

Capturing with the Nexus 5X cell phone camera burst mode, we got nineteen sequential images in each image set. Due to the LCUs we used can only turn on for 2-20 seconds and the High and Extra power mode usually cannot remain on as long

as the low power mode. In most image sets of High or Extra mode, only four of the nineteen images capture the light. Thus the number of the images in the image sets for High or Extra mode is less than those for Standard or Low mode.

- The bar graph (i) in the Figure 4.1a - 4.1f are the total intensity calculated from the images stored in JPG format (applied gamma decoding), the oversaturated (more than 0.5% of the foreground pixels are of 255 upper-bound intensity value) image sets are in yellow. Because the total intensity is normalized by dividing by the exposure time and the CheckMARC irradiance reading, the oversaturated images' pixel intensities are less than they should be, thus their bars in the graph are lower than that of images not over saturated. These oversaturated image sets will be eliminated from further analysis.

- The bar graph (ii) in the Figure 4.1a - 4.1f are the total intensity calculated from the images stored in DNG format. As same with the JPG graph, the oversaturated (more than 0.5% of the foreground pixels are of 971 (WhileLevel 1023 - BlackLevel 52) upper-bound intensity value) image sets are in yellow.

  In the figure 4.1c(ii), as marked by the orange rectangle, images underexposed are captured with $1/250s$ and $1/500s$ exposure time. Their maximum intensity is below 50 (5% of the WhiteLevel) and the 5% threshold almost treats the whole image as the light foreground resulting in their normalized total intensities being $13\% - 137\%$ higher than other image sets. So these underexposed image sets (including those DNG image sets and their corresponding JPG image sets) will be eliminated from the further calculation.

- The magenta dots in the bar graph (i) and (ii) in the Figure 4.1a - 4.1f are the maximum intensity of the image before normalized by the exposure time and the CheckMARC irradiance reading.

- The bar graph (iii) in the Figure 4.1a - 4.1f are the distance of the light center away from the image center calculated upon JPG format (width=240 pixels, height=320 pixels). Figure 4.2 shows the scatter plot of the total intensity (5% threshold) against the off-center distance. The blue dots are the images of 2018-Jan-16 and the red dots are of 2018-Mar-18. (Off-centered images are

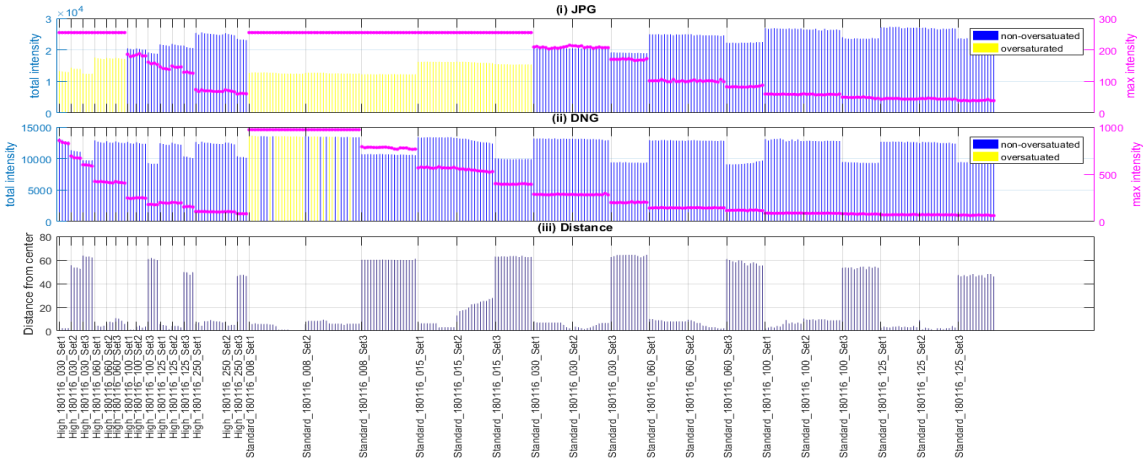

(a) LCU1_2018-Jan-16_all

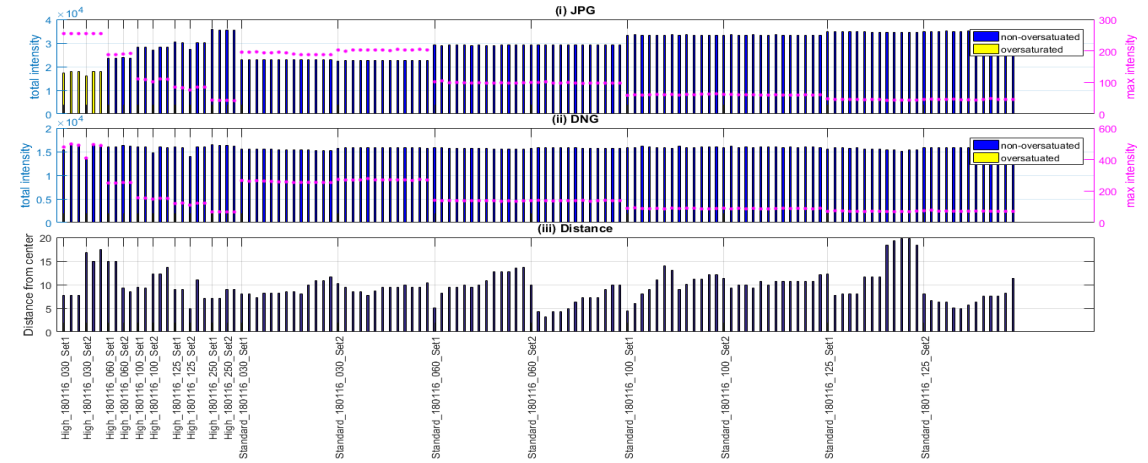

(b) LCU2_2018-Jan-16_all

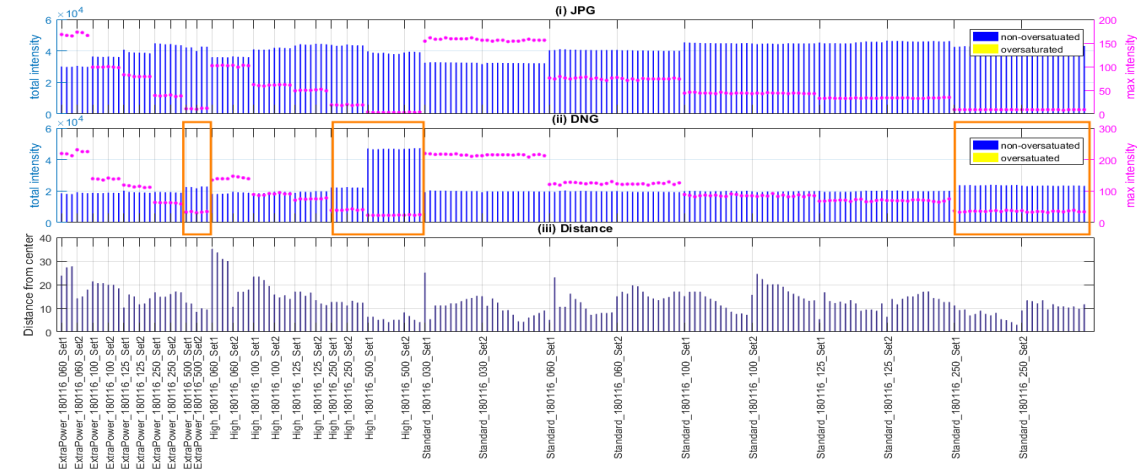

(c) LCU3_2018-Jan-16_all

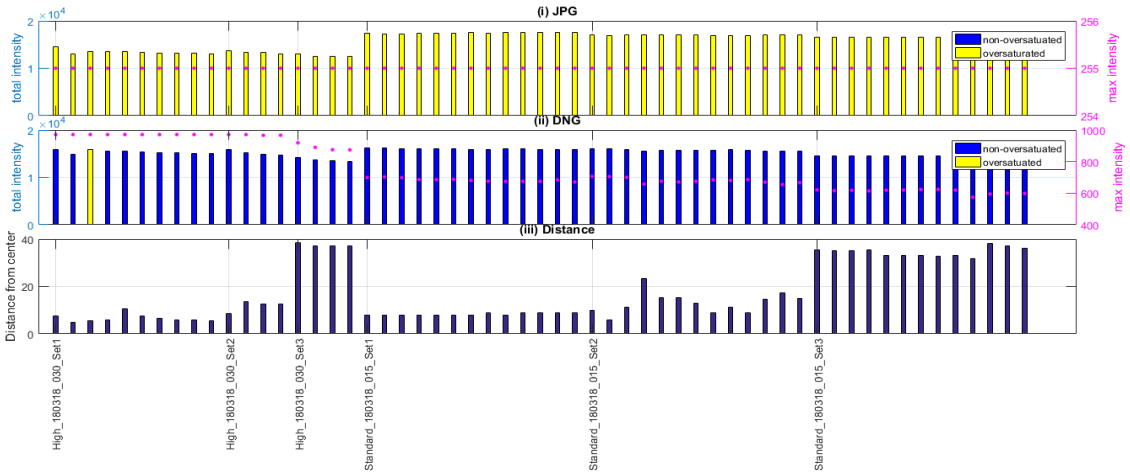

(d) LCU1_2018-Mar-18_all

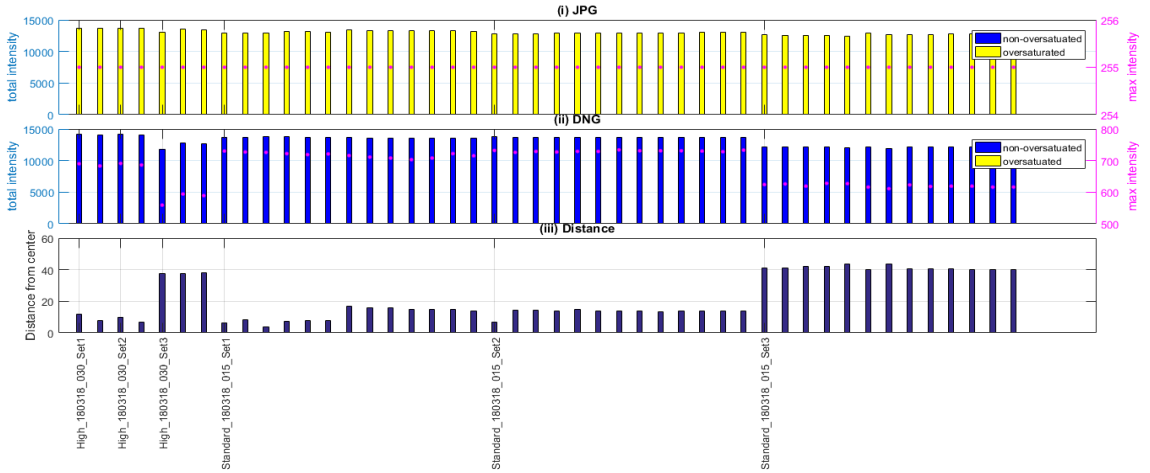

(e) LCU2_2018-Mar-18_all

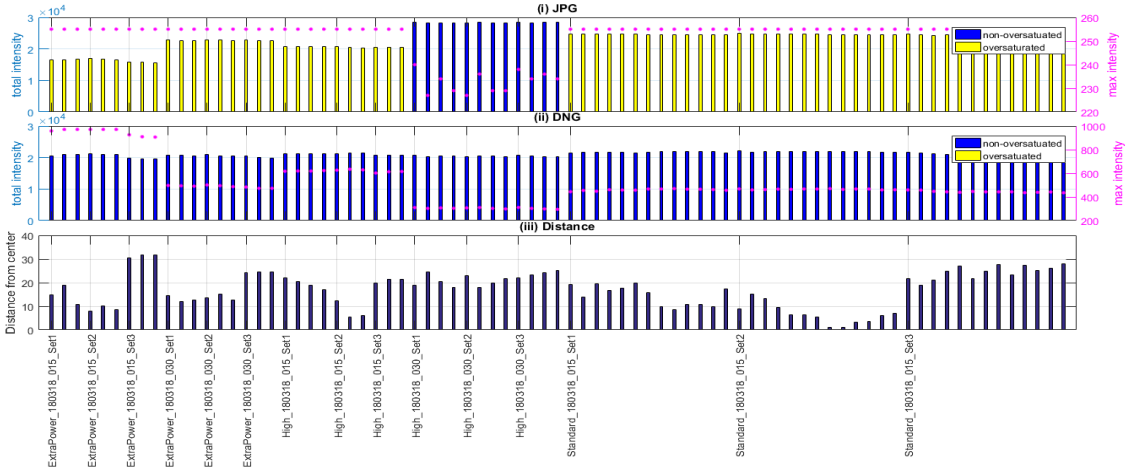

(f) LCU3_2018-Mar-18_all

Figure 4.1: Total intensity (5% threshold) and distance from center of all image sets.

only available for LCU1 on 2018-Jan-16.) As shown in Figure 4.2, the total intensity of the DNG format drops approximately 10% when the off-center distance exceeds 30. These images will be eliminated from further calculation.

Compare the image sets captured on 2018-Jan-16 and 2018-Mar-18, the variation within each date are rather smaller than the inter-day difference. As shown in Figure 4.2, compare to the image sets captured on 2018-Jan-16, those captured on 2018-Mar-18 have a larger total intensity for LCU1 and LCU3 but smaller total intensity for LCU2. If the inter-day difference is introduced by using different filter sets, different camera parameter settings or the environment light interference, the inter-day difference should appear the same trend for all the three lights used. So the difference introduced by a systematic error or the environment light between these two days does not hold. Since we only collect the CheckMARC readings once in July 2017, it is unknown if the CheckMARC can give the same value on these two dates. The reason could be some unknown differences between the curing lights used on these two dates. Therefore, further analysis will be taken upon both dates separately.

Removing the image sets over or underexposed in DNG, exceeding 30 off-center distance obtains Figure 4.3. These image sets are used for further analysis with DNG format. For the analysis with JPG format, only the non-oversaturated image sets as shown in (i) of 4.3a - 4.3f will be used.

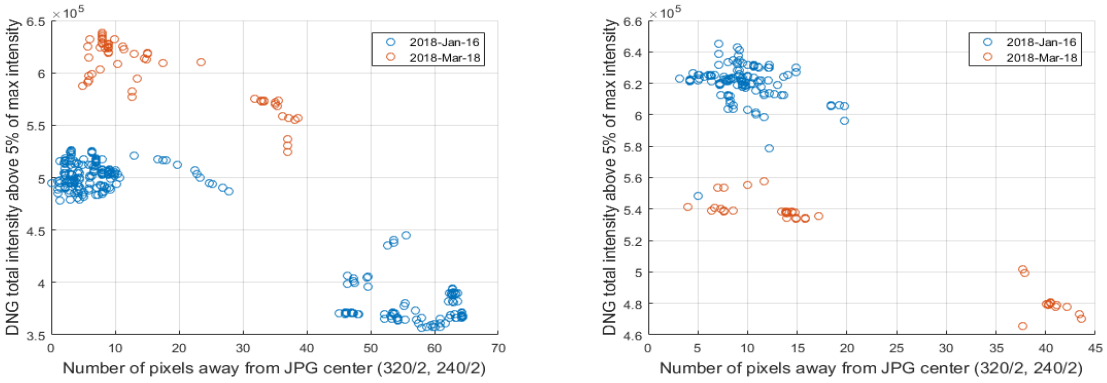

(a) LCU1

(b) LCU2

(c) LCU3

Figure 4.2: Total intensity against off center distance.

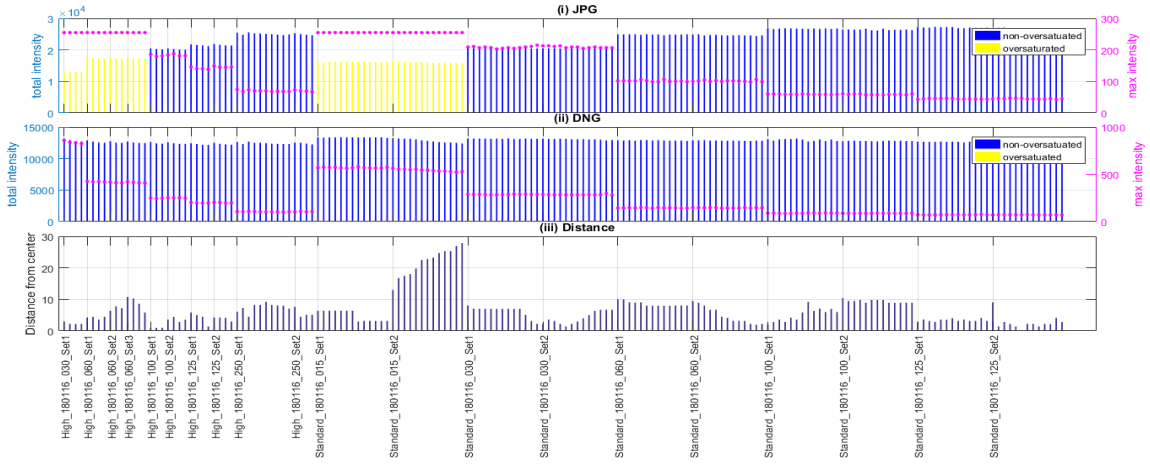

(a) LCU1_2018-Jan-16

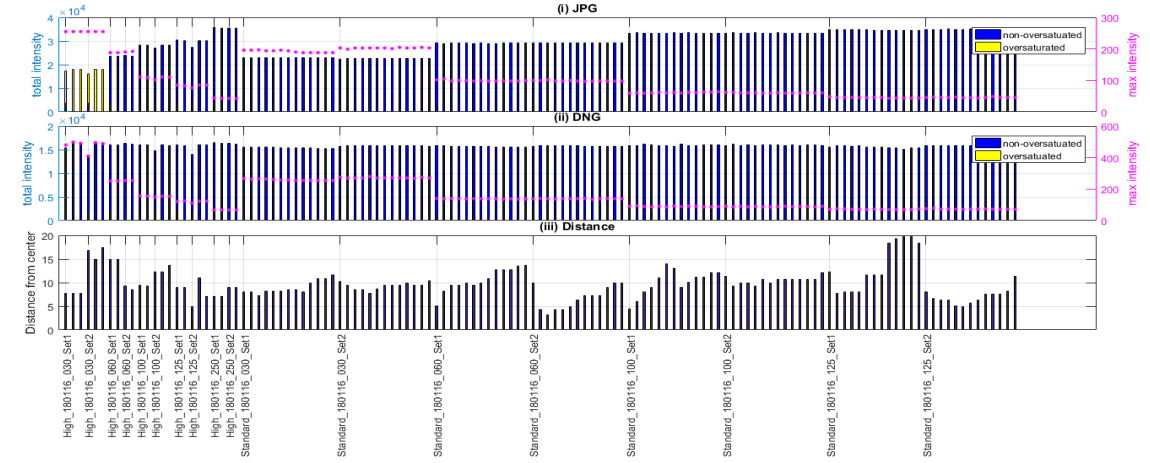

(b) LCU2_2018-Jan-16

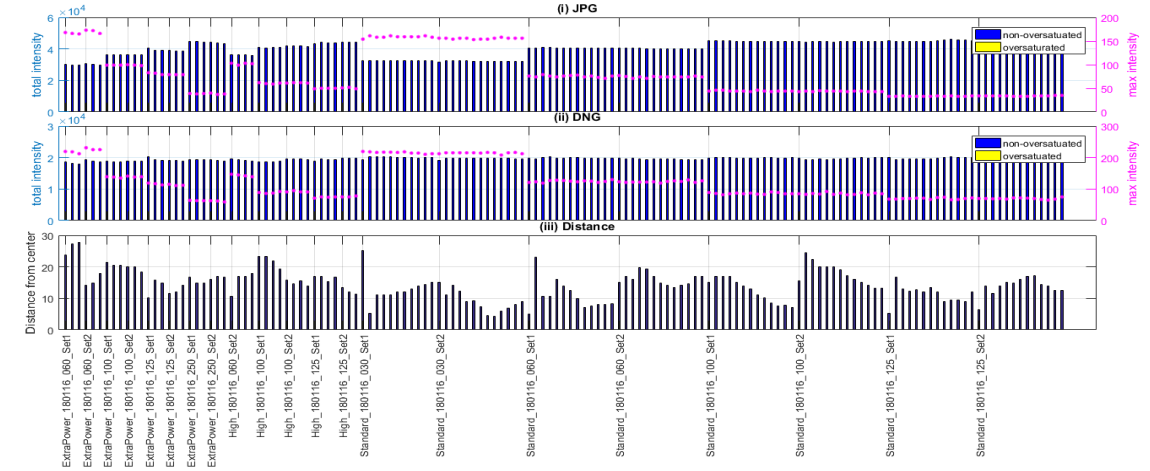

(c) LCU3_2018-Jan-16

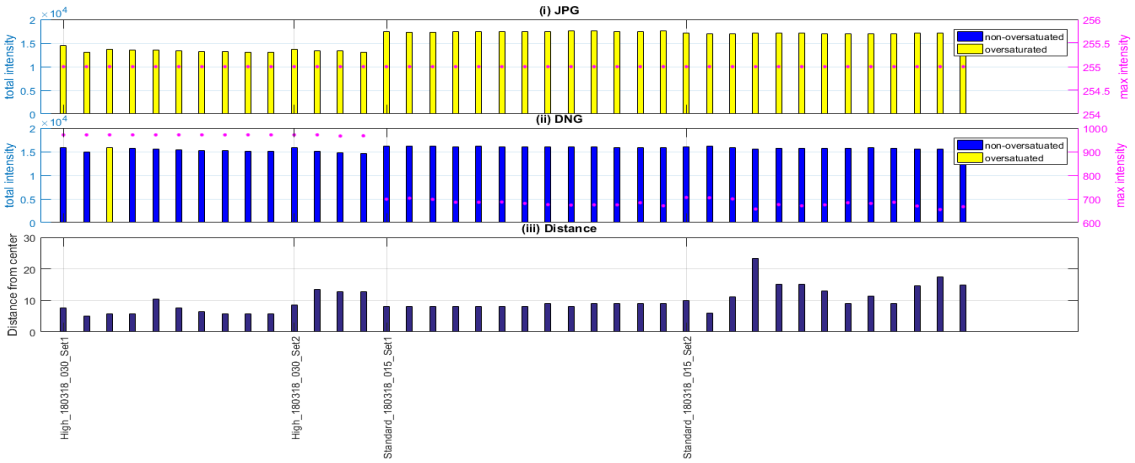

(d) LCU1_2018-Mar-18

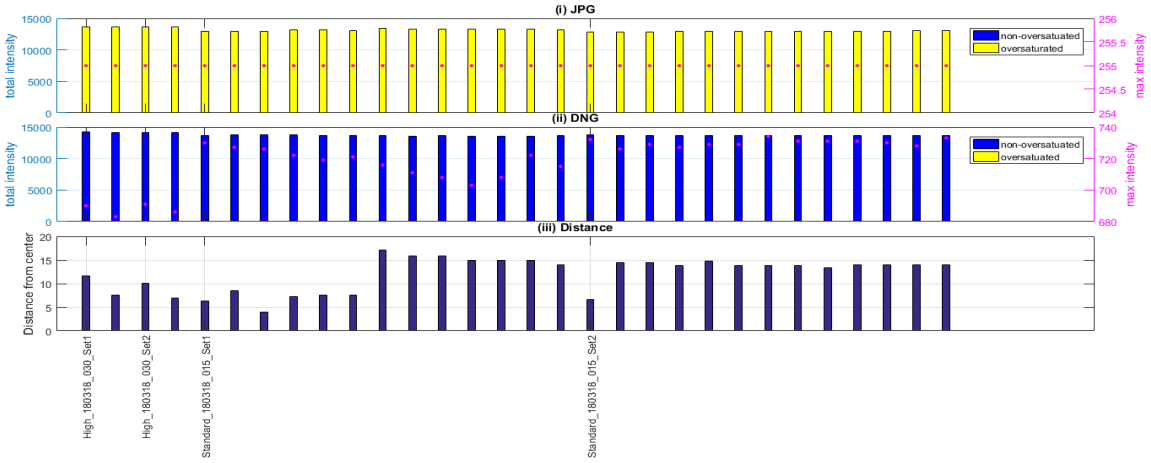

(e) LCU2_2018-Mar-18

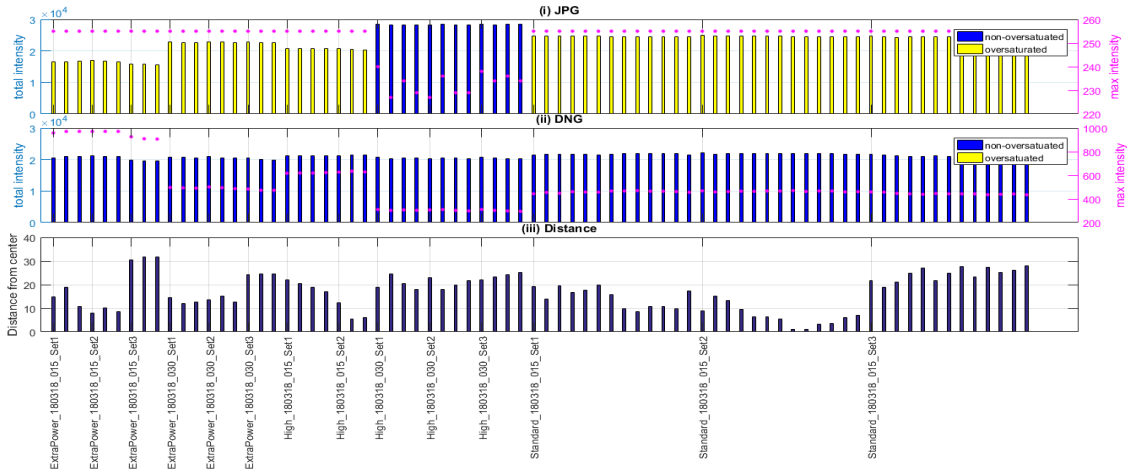

(f) LCU3_2018-Mar-18

Figure 4.3: Total intensity (5% threshold) and distance from center of image sets excluding oversatuated DNG, underexposed DNG and off-centered sets.

The burst mode and the off-center distance calculation simplify the taking of the images as we can eliminate those imperfect images and pick the best of multiple shots.

4.2 Exposure Time

After eliminating the image sets captured with the exposure time that are over or underexposed, the selected image sets are captured with exposure time from $1/15s$ to $1/250s$. To check for a certain threshold, if the longer exposure time can result in a more accurate estimation, for each curing light with each exposure time, the relative error (equation (3.2)) and overall variation (equation (3.3)) are calculated respectively.

To calculate the relative error for each exposure time as equation (3.2), the intensity_ratio is calculated with images from two image sets captured with the same exposure time for different modes of certain light. E.g. for curing light LCU3, with $1/60s$ exposure time, we captured image set s1, s2 for Standard mode, image set h1 for High mode and image set e1, e2 for ExtraPower mode. Then intensity_ratio h1/s1, h1/s2, e1/h1, e2/h1 are involved in the calculation of relative error for LCU3 with $1/60s$ exposure time.

Due to the image sets for LCU1 and LCU2 captured on 2018-Mar-18 do not have same exposure time for both high and standard modes, the relative error only calculated for the image sets captured on 2018-Jan-16 for these two lights and for LCU3 of both dates as shown in Figure 4.4. In all the four graphs, the errors for the DNG format are less than 5% for all the exposure times and with the exposure time decreases the errors is relatively stable. Due to excluding the oversaturated JPG images from the calculation, the data points on the graph of JPG format is less than that of DNG format. The errors of JPG format is larger than DNG format and appears increasing with the exposure time decreases.

Figure 4.5 shows the overall variation of the images captured with the same exposure time for a curing light. (The coefficient of variation of the total intensity above 5% threshold normalized by the CheckMARC reading is calculated over all images from the image sets captured for a curing light with the same exposure time despite different light power mode). The blue line representing the overall variation

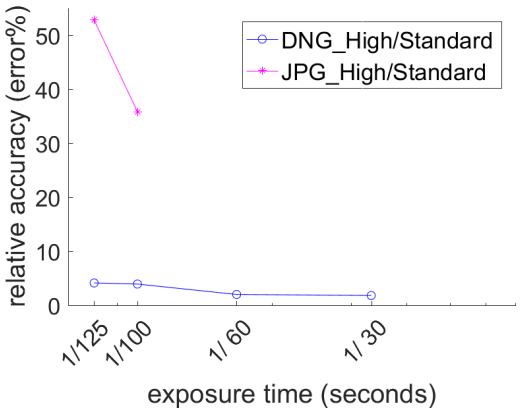

(a) LCU1 2018-Jan-16 relative error for each exposure time

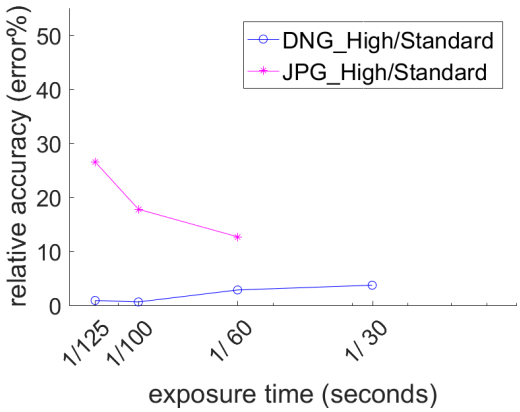

(b) LCU2 2018-Jan-16 relative error for each exposure time

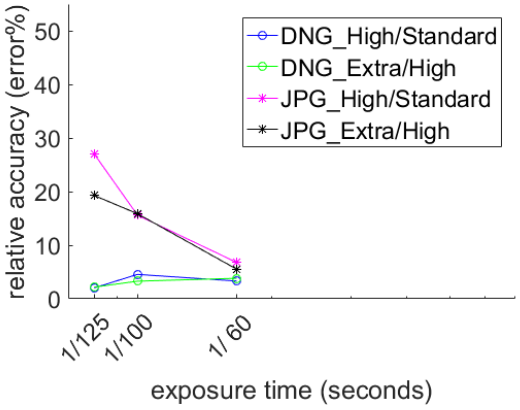

(c) LCU3 2018-Jan-16 relative error for each exposure time

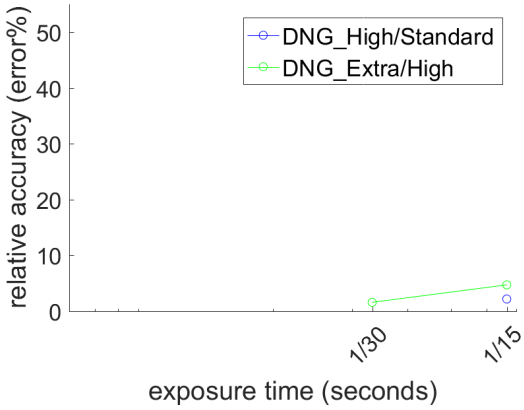

(d) LCU3 2018-Mar-18 relative error for each exposure time

Figure 4.4: Relative error for each curing light with each exposure time.

of DNG format appears flat (remaining below 5%) along with the exposure time increases. While for the JPG format, the overall variation increases as the exposure time decrease from $1/30s$ to $1/125s$. But at the exposure time of $1/250s$, the overall variation of JPG decreases to below 5% which is because after filtering out the over and underexposed image sets of the JPG format, only two image sets of this exposure time for the highest power mode remains (no image sets for the lower power modes involved in the calculation for this exposure time) and the variation of these two image sets is small. So with the 5% threshold and in the exposure time range from $1/125s$ to $1/30s$, the DNG format has a similar overall variation for different exposure time, but the longer exposure time makes a smaller overall variation for the JPG format.

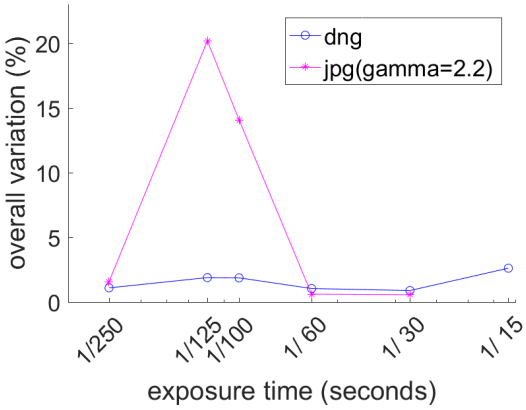

(a) LCU1 2018-Jan-16 overall variation for each exposure time

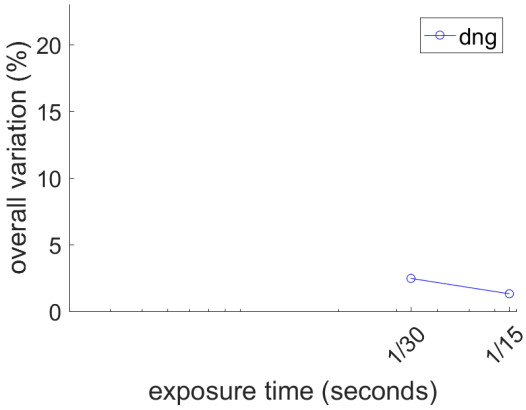

(b) LCU1 2018-Mar-18 overall variation for each exposure time

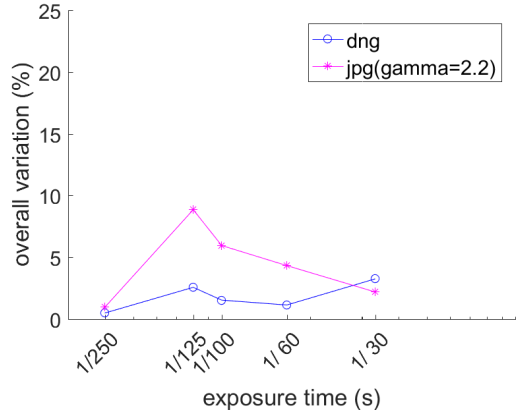

(c) LCU2 2018-Jan-16 overall variation for each exposure time

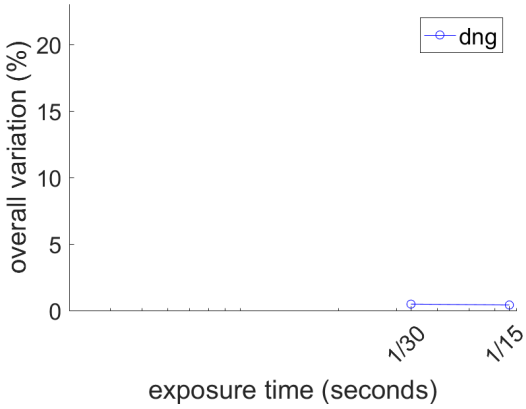

(d) LCU2 2018-Mar-18 overall variation for each exposure time

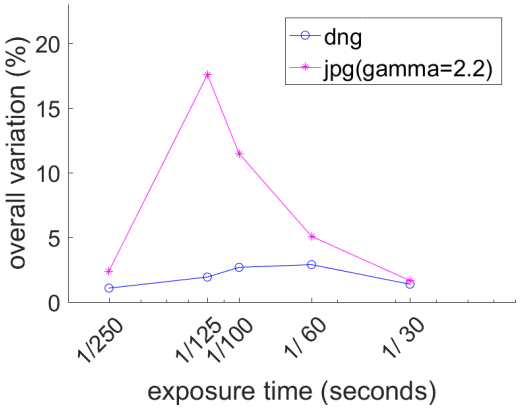

(e) LCU3 2018-Jan-16 overall variation for each exposure time

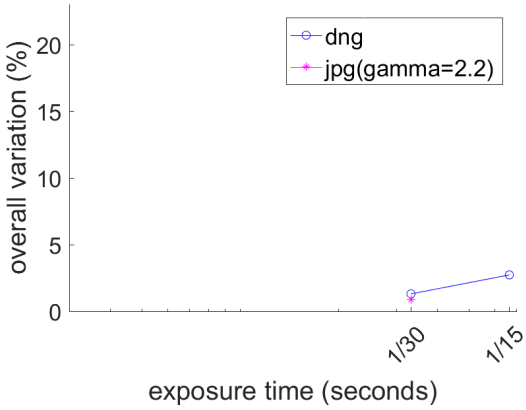

(f) LCU3 2018-Mar-18 overall variation for each exposure time

Figure 4.5: Overall variation for each curing light with each exposure time.

Without knowing the camera JPG encoding method, to analyze the reason why the relative error and the overall variation of the JPG format increase along with the exposure time decrease, different from Figure 3.6 which plots the images in one image set (with same exposure time), Figure 4.6 compares the scatter plots of the images captured on 2018-Jan-16 for the curing light LCU1 with different exposure time. The scatter plots of different exposure time distribute in the same linear range from 35 to 250 DNG value.

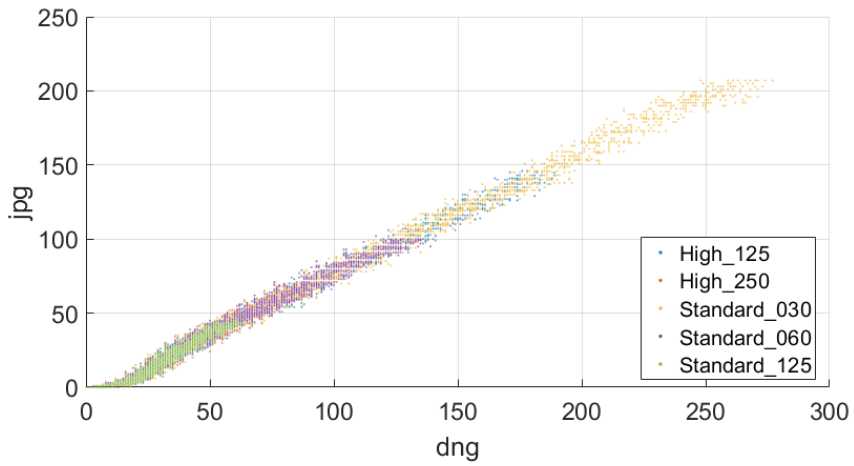

Figure 4.6: Gamma decoding (gamma=2.2) for image of different exposure time.

Figure 4.7 illustrates the pixel value mapping between JPG and DNG of all these seven images with their linear regression plot. And the colored bar illustrates the density distribution of the pixel mapping (The count of a DNG-JPG mapping pair). The more the count is, the redish the point is colored. The dense color only appears at the low end ($<$ 35 of DNG value) of the charts (Figure 4.8 amplified low end of the Standard_125) and the shorter the exposure time, the denser the low end. Compare to the linear regression plot, most points of the low end are below the linear regression line. This could cause the sum of all the pixels of JPG with shorter exposure time smaller than that with longer exposure time.

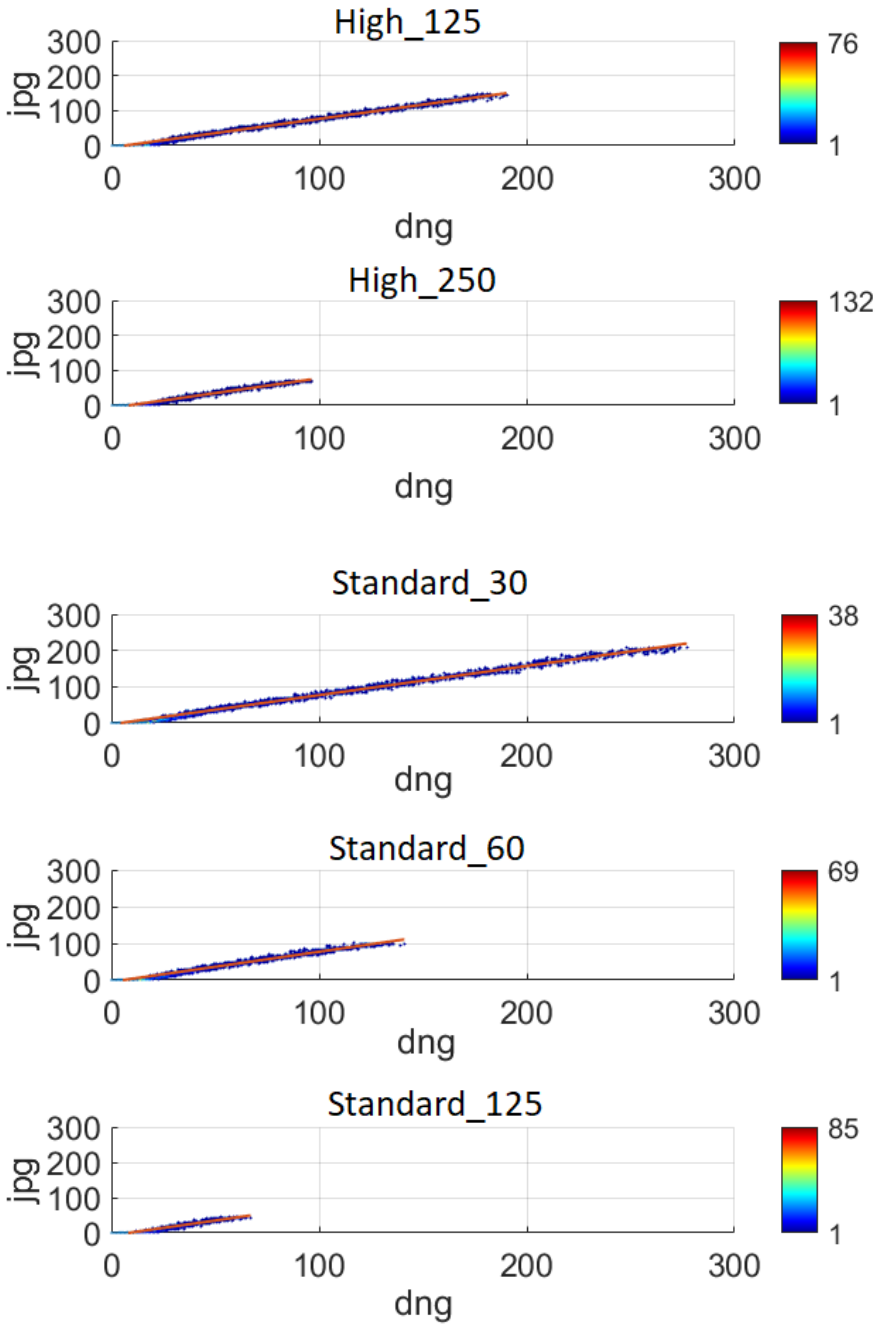

Figure 4.7: JPG-DNG scatter plot and linear regression of JPG gamma=2.2 for image of different exposure time.

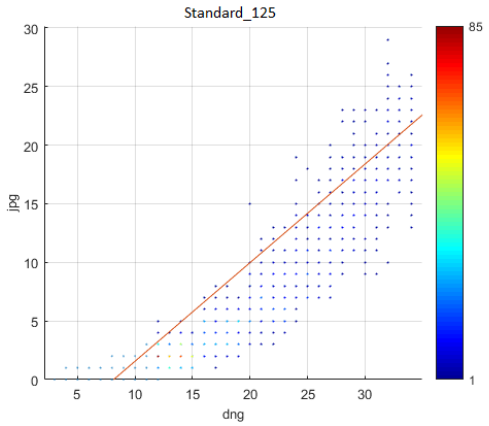

Figure 4.8: Amplified low end of the JPG-DNG scatter plot.

With regard to exposure time, DNG format(which offers a higher dynamic range) is more tolerant than JPG format. Using DNG format makes it easier to properly expose images. As we don't know exactly how JPG is generated, we have to guess a gamma value for decoding which is imperfect. Therefore the relative error and overall variation of the JPG format are larger than that of the DNG format and they increase with the exposure time decreases.

4.3 Image Size

As described in the beginning of this chapter, the size of the images is set 320×240 pixels for JPG format and 3028×4080 pixels for DNG format. Even extracted the blue channel as described in Chapter 3.1, the size of the DNG format is still more than six times as the size of JPG format. If the accuracy can be retained when reducing the DNG size, and if the time can be saved for processing a resized DNG image, then we can use the resized DNG image instead of the full-size image for further analysis. To find out if the size reduced DNG format can retain the accuracy, the DNG images are resized to the range of 1/2 to 1/32 of the DNG full size of the blue channel by using nearest-neighbor interpolation and compared to the DNG full size in terms of the relative error (equation (3.2)) and the overall variation (equation (3.3)) (Figure 4.9).

Figure 4.9 shows that for both the relative error and the overall variation, the

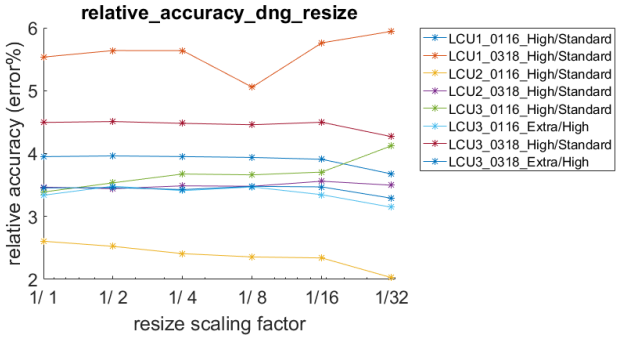

(a) Relative Error

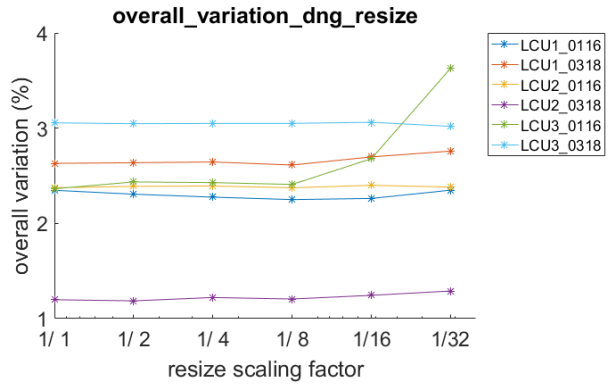

(b) Overall Variation

Figure 4.9: Comparison of different resize factor.

reducing sized DNG format (1/2 to 1/32) has no obvious decrease in accuracy compared to the full size. Processed on a laptop with Intel(R) Core(TM) i5-4210U CPU 1.79GHz, 4GB RAM, x64 Windows 10 Pro, and Matlab R2016b, the re-sample to the 1/8 full size (nearest to the JPG size) takes about 0.15-0.2 seconds for each image, but reduce the relative DNG processing time from 0.4-0.6 seconds to 0.15-0.2 seconds per image. Thus the reduced size DNG image can save the total processing time by approximate 1/3 without reducing the accuracy.

But with our version of Android which cannot fully support processing DNG images, transferring images to a laptop instead of do all the computations on the phone is inconvenient and the the operators are unable to get the results in time thus the motivation for using JPG.

4.4 Intensity Threshold Selection

Since the reduced DNG size has similar accuracy as the full size, to convenient further comparison with the JPG format, the comparison among the intensity thresholds for the foreground/background separation is based on the re-sampled DNG to the size of the JPG format.

Figure 4.10 and Figure 4.11 compare the threshold from 0% (not excluding background at all) to 30% of the maximum intensity in terms of the relative error (Equation 3.2) and the overall variation (Equation 3.3). The image sets involved in the calculation are all the image sets taken for an LCU on a single day with eliminating those overexposed, underexposed and off-centered as shown in Figure 4.3. There are fewer image sets taken on 2019-Mar-18 than that taken on 2019-Jan-16, and there are fewer non-oversaturated image sets of JPG format than that of DNG format.

Both Figure 4.11a and Figure 4.10a show that for DNG format, except 0% and 2%, plot lines are almost flat and the relative error are all below 6%; the overall variation are all below 4%. At the 0% and 2% threshold, the image sets taken on 2018-Jan-16 have much more errors (in relative error and overall variation) than other thresholds while image sets taken on 2018-Mar-18 do not. As shown in the Figure 3.2 and Figure 3.3, the background total intensity is not neglectable, and when the threshold is below 5%, it cannot separate the foreground from the background for

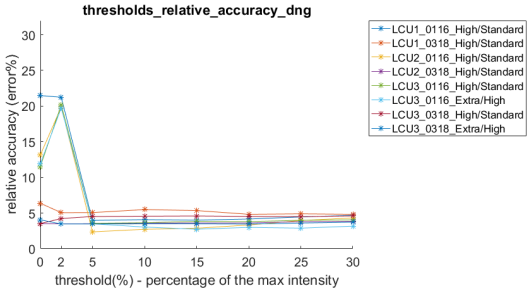

(a)

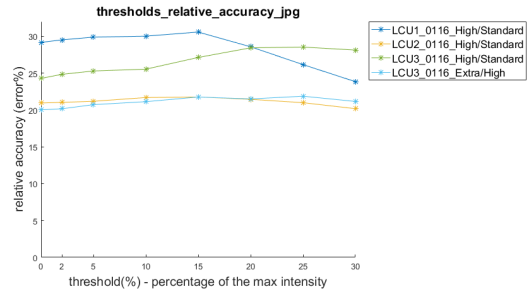

(b)

Figure 4.10: Relative error of different intensity threshold.

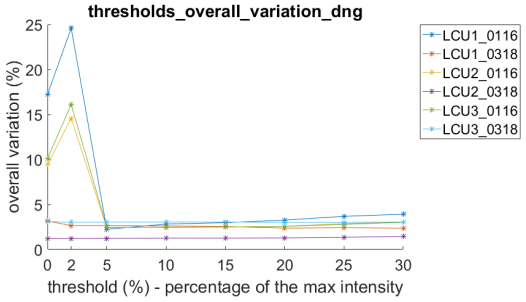

(a)

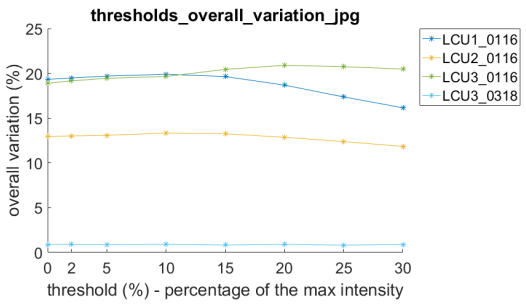

(b)

Figure 4.11: Overall variation of different intensity threshold.

the shorter the exposure time as good as for the longer exposure time. On 2018-Jan-16 image sets are taken with $1/15s$, $1/30s$, $1/60s$, $1/100s$, $1/125s$, and $1/250s$ exposure time while on 2018-Mar-18, the image sets are only taken with $1/15s$ and $1/30s$ exposure time, so involving the whole background pixels in the calculation of the normalized total intensity has much less impact on the image sets taken with long exposure times than those with shorter exposure times.

Figure 4.10b and Figure 4.11b calculate the relative error and the overall variation for the JPG format. In which LCU1_0318 and LCU2_0318 are not shown due to all the image sets of LCU1 and LCU2 taken on 2018-Mar-18 are oversaturated. And because only three image sets taken for the high mode of LCU3 on 2019-Mar-18 with exposure time $1/30s$ are not oversaturated, the plot LCU3_0318 does not show in Figure 4.10b and has much less error than other three plots in Figure 4.11b. Unlike DNG format, the relative error and the overall variation of 0% and 2% thresholds for the JPG format do not have much difference compared to other thresholds but the errors are all above 20% in the relative error and 10% in the overall variation.

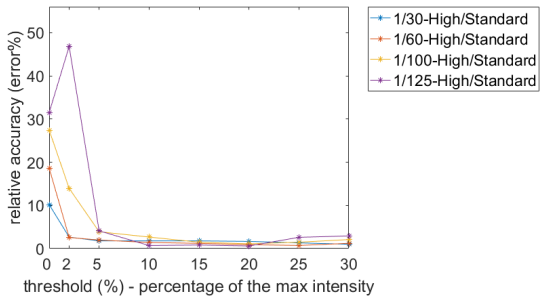

(a) LCU1 2018-Jan-16 DNG relative error

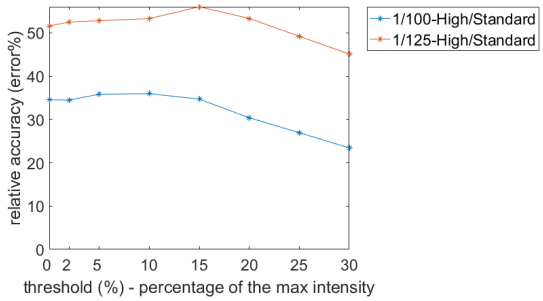

(b) LCU1 2018-Jan-16 JPG relative error

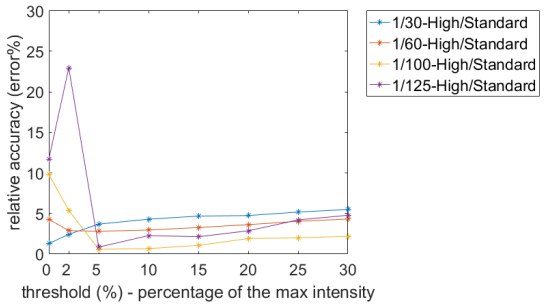

(c) LCU2 2018-Jan-16 DNG relative error

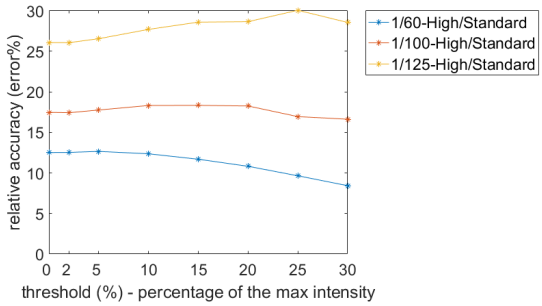

(d) LCU2 2018-Jan-16 JPG relative error

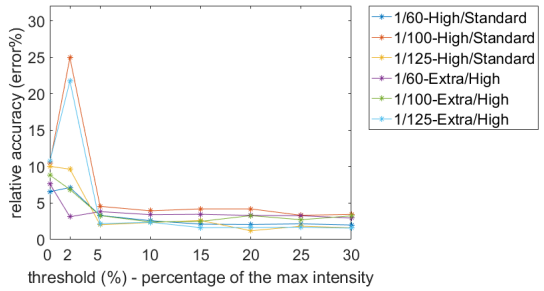

(e) LCU3 2018-Jan-16 DNG relative error

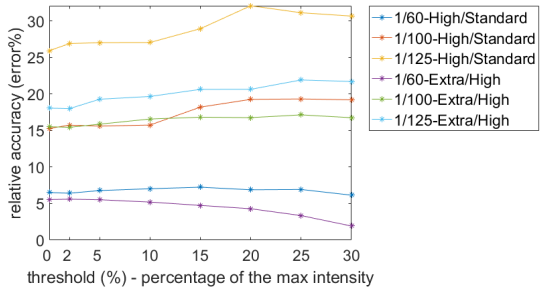

(f) LCU3 2018-Jan-16 JPG relative error

Figure 4.12: Relative error of different intensity threshold for different exposure time.

Figure 4.12 and Figure 4.13 show the relative error and the overall variation of the image sets of different exposure time with different thresholds. From which we can see that for the DNG format, the relative accuracy and the overall variation do not have much impact by different exposure time; But for the JPG format, both the relative accuracy and the overall variation have a positive correlation with the exposure time. (Except $1/250s$ exposure time which has small error because only two image sets taken for the highest power mode of these three LCUs are involved in the calculation for this exposure time.)

With regard to threshold, DNG format is more sensitive when the threshold $< 5\%$. When including all background pixels in the total intensity calculation, the error of DNG format can be 3-4 times than excluding the background pixels by the threshold $5\% - 30\%$ of the maximum pixel intensity. But between $5\% - 30\%$, the accuracy is at the same level. JPG format appears relatively stable in accuracy with the threshold between 0% and 30% for a certain exposure time. If only consider the exposure times that neither result in overexposed images for the high mode nor underexposed images for the low mode, then the smallest relative error and the overall variation of the JPG format are of the images with $1/60s$ exposure time, but still larger than that of the corresponding DNG format.

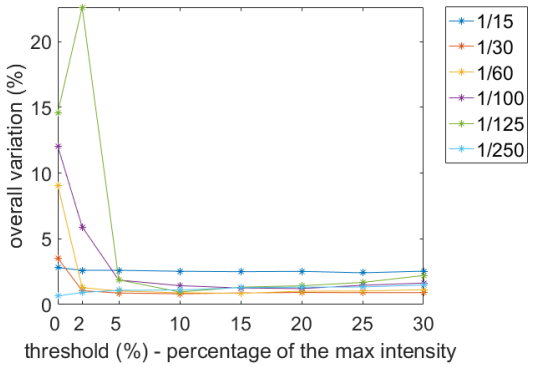

(a) LCU1 2018-Jan-16 DNG overall variation

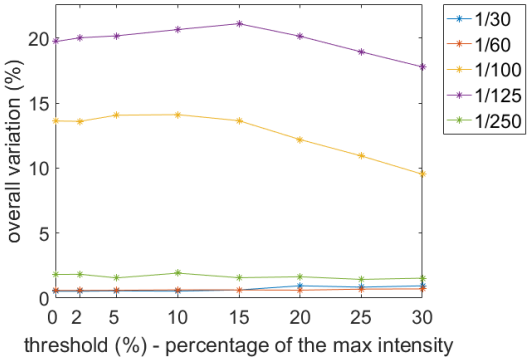

(b) LCU1 2018-Jan-16 JPG overall variation

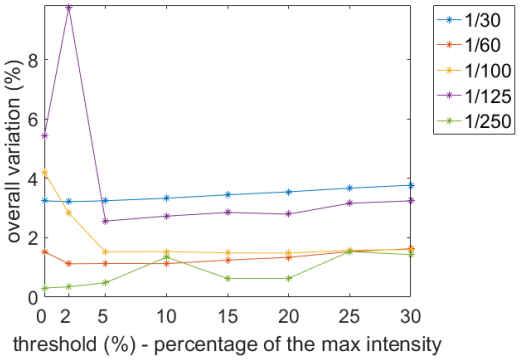

(c) LCU2 2018-Jan-16 DNG overall variation

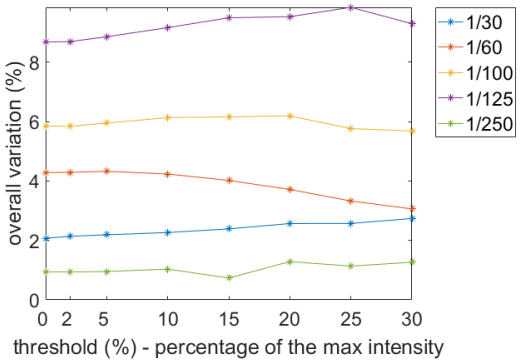

(d) LCU2 2018-Jan-16 JPG overall variation

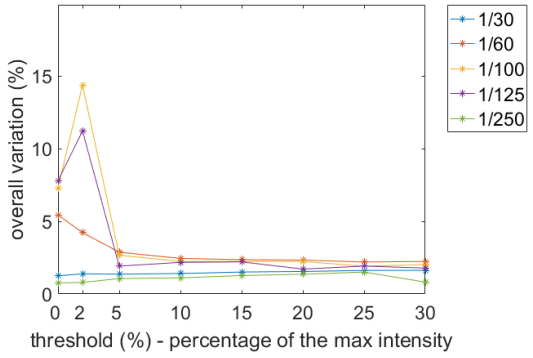

(e) LCU3 2018-Jan-16 DNG overall variation

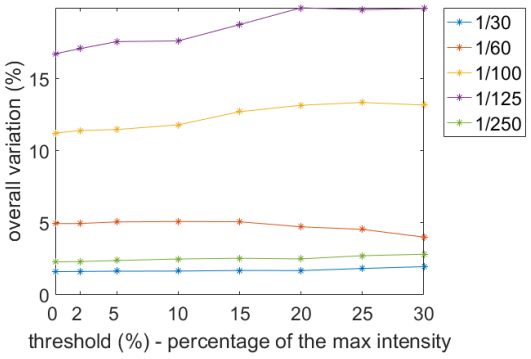

(f) LCU3 2018-Jan-16 JPG overall variation

Figure 4.13: Overall variation of different foreground/background separating threshold for different exposure time.

4.5 Verification

This section will use a set of images captured on 2018-Mar-21 that did not involved in the preceding sections and contains two more LCUs than the image sets used in preceding sections to verify if the conclusions made out of the three LCUs used in preceding sections can also apply to other LCUs. And in addition, because captured with the auto-capture algorithm mentioned in Section 2.3, the exposure time of the images in this set may be set more properly. In the preceding sections, when comparing different exposure times, the images captured with same exposure time for different power modes are put together to calculate relative error. The exposure time proper for higher mode may not proper for lower mode. So with the images used in this section, we can verify if a more proper exposure time results in a higher accuracy of JPG format.

The set of images adopted in this section was originally used by D'silva in [2] to estimate the light's power with JPG format without applying gamma decoding. The images were captured without camera burst mode. For two power modes of a LCU, one image was captured for the higher mode and one image was captured for the lower mode to form a pair. Five such image pairs were captured for each LCU except LCU3 which has three power modes thus five image pairs for each two modes combination. In this thesis, I reorganize the images in the image pairs of each LCU to put all the images for each mode as an image set. Thus, except for LCU3 which has ten images for ExtraPower, High and Standard mode respectively, every other curing light has five images for the High mode and five images for the Standard (or Low) mode. Figure 4.14 shows the total intensity of the DNG format resized to the size of JPG format and normalized by the exposure time and the CheckMARC reading, the total intensity of JPG format applied gamma=2.2 decoding and the distance the light center away from the image center. There are no underexposed or off-centered images but an overexposed image set of LCU6, thus this image set will be eliminated from the calculation of the relative error and the overall variation. Figure 4.10 and Figure 4.11 show that when the intensity threshold in the range of $5\% - 30\%$ both the relative accuracy and the overall variation are stable. So 30% threshold is used in this section.

Calculating the Equation 3.2 and Equation 3.3 upon all the bars in Figure 4.14

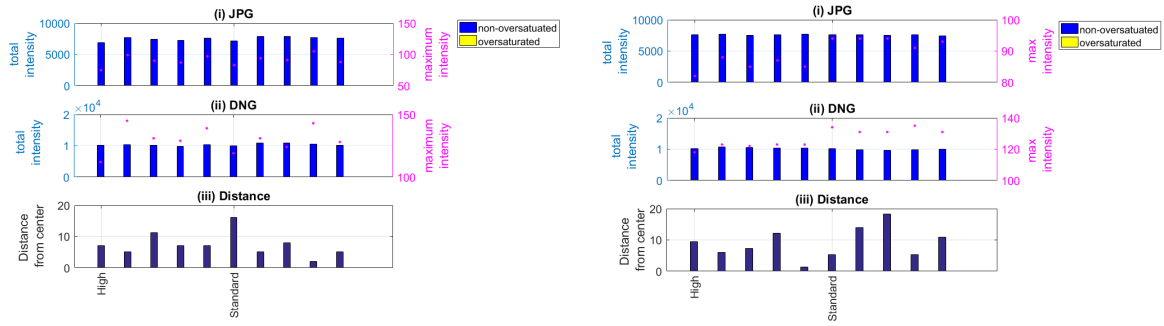

(a) LCU1_2018-Mar-21

(b) LCU2_2018-Mar-21

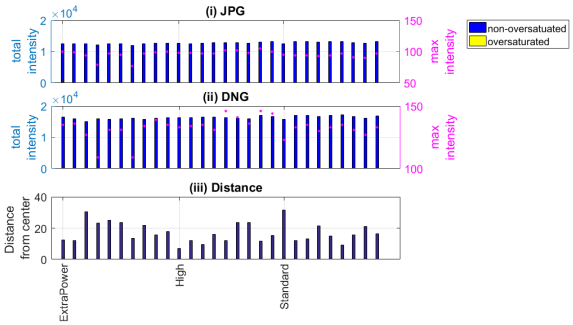

(c) LCU3_2018-Mar-21

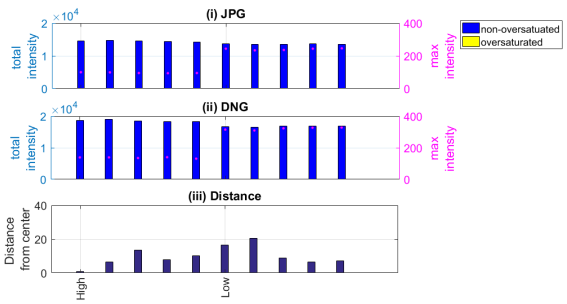

(d) LCU4_2018-Mar-21

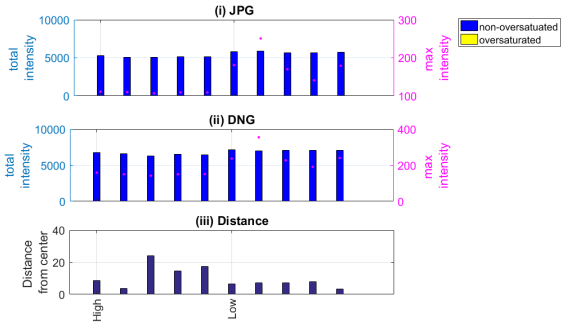

(e) LCU5_2018-Mar-21

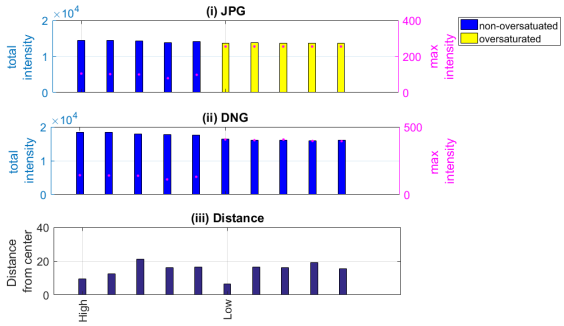

(f) LCU6_2018-Mar-21

Figure 4.14: Total intensity (30% threshold) and distance from center.

get us the results in Table 4.2. The relative error of the JPG format of LCU6 is N/A and its JPG overall variation is much smaller than that of DNG because all its JPG images for the low mode are eliminated from calculation due to overexposed but their corresponding DNG format images are still involved in the calculation.

Table 4.2: Accuracy on 2018-Mar-21 image sets.

Light	**overall variation (%)**		**Relative Error (%)**		
	DNG	JPG		DNG	JPG
LCU1	3.39	4.44	High/Standard	4.25	3.90
LCU2	3.31	1.05	High/Standard	6.30	0.33
LCU3	3.00	2.62	High/Standard	3.06	2.37
			ExtraPower/High	2.74	2.31
LCU4	5.60	3.47	High/Standard	10.20	6.83
LCU5	4.62	6.10	High/Low	7.38	10.36
LCU6	6.04	1.87	High/Low	11.32	N/A

Unlike Figure 4.12 and Figure 4.13, in which the images captured with same exposure time for different power modes are evaluated together, the relative error of the JPG format being larger than the error of the corresponding DNG format even for the case of $1/60s$ exposure time that the error is the smallest among other exposure time considered, the calculation in this section uses the images with different exposure time more proper for different light power mode and as shown in Table 4.2, the relative error of the JPG format achieves comparable accuracy with the DNG format.

Chapter 5

CONCLUSION AND FUTURE WORK

5.1 Conclusion

In this thesis, we have evaluated the accuracy of estimating the curing light degradation with cell phone images. By analyzing the images taken for different LCUs with different exposure time in DNG and JPG format and comparing to the CheckMARC readings, we conclude that the measurements of relative intensity differ from the corresponding relative measurements using CheckMARC by no more than 12%. Thus cell phone application can be a supplement to the CheckMARC service.

Taking a sequential burst capture of images potentially improves the accuracy in cases where the alignment of the light or the capturing moment is less than perfect. By removing the images where the light center significantly shifts away from the image center and picking the median value of each burst image set, the imperfect images could be eliminated.

DNG is preferable to JPG as we don't know exactly how JPG is generated (does image sensor apply any operations at hardware level, what image processing steps are involved in the pipeline, which compression method is picked and what parameters are used are all unknown to us) and therefore need to guess a gamma value, which results in an imperfect decoding. And DNG (which offers a higher dynamic range) is more tolerant than JPG with regard to exposure time, thus makes it easier to properly expose images. However, there are limitations of using the DNG format. Although decreasing the image size doesn't result in a loss of accuracy and it is quicker to do DNG re-sizing than JPG decoding, it still takes time in image preprocessing on DNG format for image analysis, and not all Android cell phones support saving or processing images in DNG format and current lack of software support for DNG images.

The JPG format is supported by all Android cell phone. Without knowing how the camera generates JPG image, we guess a gamma value (gamma=2.2) and applied

decoding (which is imperfect) upon the JPG format. The non-oversaturated JPG image shows a linear relationship with DNG format when the DNG pixel intensity in the range of 35 to 250. Below 35, the JPG pixel intensity tends to be lower than the linear regression line. This result in the accuracy of the JPG format decreases when the exposure time decreases. But with proper exposure time for all the images involved in the calculation, the deviations from linear in Figure 4.6 are rather inconsequential and JPG can result in comparable accuracy as that of DNG format.

The separation of foreground from background is a seemingly significant issue, as intensity measurements are quite sensitive to the choice of threshold and a clear boundary doesn't exist. However, when considering relative measurements the choice of threshold becomes rather uncritical, provided that it is not chosen all too small and the images aren't underexposed ($5\% - 30\%$ threshold).

5.2 Future Work

We recommend future work in the following aspects:

- As explained in Section 4.1, due to some unknown reason the inter-day difference between the image sets taken on 2018-Jan-16 and 2018-Mar-18 is much larger than the intra-day difference. We only collect the CheckMARC readings once in July 2017 as a baseline to evaluate the accuracy of using the total intensity of the image to estimate the LCU's degradation. Without knowing the CheckMARC readings collected on these two dates, this thesis calculates the accuracy within each date. In the future, more extensive testing is needed. E.g. we could consider getting the CheckMARC readings for each date that we collect the cell phone images and do the inter-day comparison.

- In this thesis, we only use one cell phone - Nexus 5X to collect the images of the LCU. In the future, different cell phones could be involved to collect images and considering they may use different JPG encoding methods, we may use different methods to process JPG images and evaluate the accuracy of different cell phones.

Bibliography

[1] Ana I. Barbosa, Poonam Gehlot, Kalpita Sidapra, Alexander D. Edwards, and Nuno M. Reis. "Portable smartphone quantitation of prostate specific antigen (PSA) in a fluoropolymer microfluidic device". In: *Biosensors and Bioelectronics* 70 (2015), pp. 5–14.

[2] Bryan Thomas D'silva. "An Android application for low-cost efficacy monitoring of dental curing lights". M.A.C.Sc. report. Halifax, NS: Dalhousie University, 2018.

[3] Khalid A. Ghuzlan, Mohammed T. Obaidat, and Mai M. Alawneh. "Cellular-phone-based computer vision system to extract shape properties of coarse aggregate for asphalt mixtures". In: *Engineering Science and Technology, an International Journal* 22.3 (2019), pp. 767–776.

[4] Dan B. Goldman. "Vignette and exposure calibration and compensation". In: *IEEE Transactions on Pattern Analysis and Machine Intelligence* 32.12 (Dec. 2010), pp. 2276–2288.

[5] Rafael C. Gonzalez and Richard E. Woods. *Digital Image Processing, Third Edition*. Pearson, 2008.

[6] Suvardhan Kanchi, Myalowenkosi I. Sabela, Phumlane Selby Mdluli, Inamuddin, and Krishna Bisetty. "Smartphone based bioanalytical and diagnosis applications: A review". In: *Biosensors and Bioelectronics* 102 (2018), pp. 136–149.

[7] Norbert Krämer, Ulrich Lohbauer, Franklin Garcia-Godoy, and Roland Frankenberger. "Light curing of resin-based composites in the LED era". In: *American Journal of Dentistry* 21.3 (2008), pp. 135–142.

[8] Anna Mangat, Anil Dhingra, and Gaurav Bhardwaj. "Curing Lights and the science behind them - An Overview". In: *Journal of Dental and Medical Sciences* 13.12 Ver.IV (2014), pp. 35–39.

[9] Miguel G. Neumann, Carla C. Schmitt, Giovana C. Ferreira, and Ivo C. Corrêa. "The initiating radical yields and the efficiency of polymerization for various dental photoinitiators excited by different light curing units". In: *Dental Materials* 22.6 (2006), pp. 576–584.

[10] Jun Ohta. *Smart CMOS Image Sensors and Applications*. CRC Press, 2017.

[11] Helton Jader Souza de Oliveira, Pedro Lemos de Almeida, Bárbara Araújo Sampaio, Julys Pablo Atayde Fernandes, Osmundo Dantas Pessoa-Neto, Eduardo Antônio de Lima, and Luciano Farias de Almeida. "A handheld smartphone-controlled spectrophotometer based on hue to wavelength conversion for molecular absorption and emission measurements". In: *Sensors and Actuators B: Chemical* 238 (2017), pp. 1084–1091.

[12] Richard B. Price, Daniel Labrie, Sonya Kazmi, John Fahey, and Christopher M. Felix. "Intra- and inter-brand accuracy of four dental radiometers". In: *Clinical Oral Investigations* 16.3 (2012), pp. 707–717.

[13] Richard B. Price, Adrian C. Shortall, and William M. Palin. "Contemporary issues in light curing". In: *Operative Dentistry* 39.1 (2014), pp. 4–14.

[14] Frederick A. Rueggeberg. "State-of-the-art: Dental photocuring - A review". In: *Dental Materials* 27.1 (2011), pp. 39–52.

[15] Joonchul Shin, Seoyeon Choi, Jung-Sik Yang, Jaewoo Song, Jong-Soon Choi, and Hyo-Il Jung. "Smart Forensic Phone: Colorimetric analysis of a bloodstain for age estimation using a smartphone". In: *Sensors and Actuators B: Chemical* 243 (2017), pp. 221–225.

[16] Adrian C. Shortall, Christopher J. Felix, and David C. Watts. "Robust spectrometer-based methods for characterizing radiant exitance of dental LED light curing units". In: *Dental Materials* 31.4 (2015), pp. 339–350.

[17] Zachary J. Smith, Kaiqin Chu, Alyssa R. Espenson, Mehdi Rahimzadeh, Amy Gryshuk, Marco Molinaro, Denis M. Dwyre, Stephen Lane, Dennis Matthews, and Sebastian Wachsmann-Hogiu. "Cell-phone-based platform for biomedical device development and education applications". In: *PloS one* 6.3 (2011).

[18] G. K. Wallace. “The jpeg still picture compression standard”. In: *IEEE Transactions on Consumer Electronics* 38.1 (1992), pp. xviii–xxxiv.

[19] Daniel Whiteson, Michael Mulhearn, Chase Shimmin, Kyle Cranmer, Kyle Brodie, and Dustin Burns. “Searching for ultra-high energy cosmic rays with smartphones”. In: *Astroparticle Physics* 79 (2016), pp. 1–9.